Structure of $N = 56$ isotones with $36 \leqslant Z \leqslant 42$ protons

J. Wiśniewski,[1] W. Urban,[1] T. Rząca-Urban,[1] K. Sieja,[2,3] A. Blanc,[4] M. Jentschel,[4] C. Micheagnoli,[4] P. Mutti,[4] U. Köster,[4] G. de France,[5] G. S. Simpson,[6] and C. A. Ur[7]

[1]*Faculty of Physics, University of Warsaw, PL-02-093 Warsaw, Poland*
[2]*Université de Strasbourg, IPHC, Strasbourg, France*
[3]*CNRS, UMR7178, 67037 Strasbourg, France*
[4]*Institut Laue-Langevin, Grenoble, France*
[5]*Grand Accélérateur National d'Ions Lourds (GANIL), CEA/DSM - CNRS/IN2P3, Bd Henri Becquerel, BP 55027, F-14076 Caen Cedex 5, France*
[6]*LPSC, Université Joseph Fourier Grenoble 1, CNRS/IN2P3, Institut National Polytechnique de Grenoble, F-38026 Grenoble Cedex, France*
[7]*INFN, Legnaro, Italy*

(Received 14 March 2023; revised 11 May 2023; accepted 21 July 2023; published 8 August 2023)

Excited levels in ^{92}Kr, ^{96}Zr, and ^{98}Mo nuclei were reinvestigated using high-statistics multiple-γ coincidence data measured with the EXILL and FIPPS Ge arrays, following neutron-induced fission of ^{235}U and neutron capture on a ^{97}Mo target, respectively. The experimental goal was to search for new levels, especially with low spins, as well as to firm up spin-parity assignments to known levels. In total of 16 new levels with 64 new or corrected decays and 35 new or improved spin-parity assignments were observed in the three nuclei. We also performed large-scale shell-model calculations to learn more about the microscopic structure of levels in these nuclei. The evolution of collectivity in $N = 56$ isotones is discussed, stressing the important role of various single-particle excitations, in particular of the $\pi g_{9/2}$ orbital, in the shape evolution in the region.

DOI: 10.1103/PhysRevC.108.024302

I. INTRODUCTION

The spectacular shape evolution of neutron-rich nuclei in the mass $A \approx 100$ region has provided for several decades prime information on the nature of low-energy nuclear excitations, helping us to understand nuclear collectivity, a phenomenon emerging in a finite quantum system. This evolution has been studied in great detail as a function of the neutron number, N, above the $N = 50$ shell closure, revealing basic mechanisms driving the shape change around $N = 59$. The evolution along N was recognized as being due to the population of the deformation-driving, low-Ω orbitals originating from the $h_{11/2}$ neutron shell [1–5], helped by the $9/2^+[404]$ neutron extruder [6,7].

The nuclear deformation is, primarily, a result of the proton-neutron interaction [8,9]. In the $A \approx 100$ region it involves low-Ω orbitals emerging from the $h_{11/2}$ neutron and the $g_{9/2}$ proton shells. The population of the neutron orbitals, helped by the catalytic action of the $9/2^+[404]$ extruder, was discussed in recent works [10,11]. Less is known about the mechanism behind the population of the $g_{9/2}$ proton shell in the region.

Above $N = 56$ there is a rapid increase of collective effects due to the growing neutron number [5,12]. To study the population of the $g_{9/2}$ proton shell, one should minimize the contribution of neutrons to the collectivity evolution in the region. Therefore, the $N = 56$ isotonic line may be the right place to look for the evolution of collective effects due to the population of the $\pi g_{9/2}$ shell.

Figure 1 shows the density of levels observed (to date) in $N = 56$ isotones as a function of the excitation energy up to 4.2 MeV, in bins of 200 keV (the inset shows the total number of levels in this energy range; points at $Z = 46$ and 48 were added to stress the increased density in ^{98}Mo and ^{100}Ru). One observes a sudden increase of the density (and of the total number) between $Z = 40$ and $Z = 42$. It is of interest to understand whether and how this increase is related to the population of the $\pi g_{9/2}$ shell above 2 MeV, what is the mechanism of this population, and whether these numerous levels contribute to an emergence of collective effects at $N = 56$.

In the past the spin-orbit-partner (SOP) mechanism was proposed [14,15] to explain the sudden increase of the ground-state deformation in Sr and Zr isotopes. However, the monopole interaction between the $\nu g_{7/2}$ and $\pi g_{9/2}$ spin-orbit partners extends over a range of neutrons too wide to explain the observed suddenness of the deformation change at $N = 59$. Furthermore, it does not address the role of the $\nu h_{11/2}$ shell [10].

As seen in Fig. 1, in ^{98}Mo there are two "maxima" in the level density, around 2.5 and 3.3 MeV. In ^{100}Ru they overlap into one centered around 2.9 MeV. This observation relates to the level systematics shown in Fig. 6 of Ref. [10], where two sets of levels, corresponding to two different proton structures, overlap in energy in isotopes with $Z = 42$ and $Z = 44$ but not in isotopes with other Z numbers. At $N = 56$ one expects two different neutron structures, namely levels related to the population of the $\nu d_{5/2}$ shell and higher-lying levels related

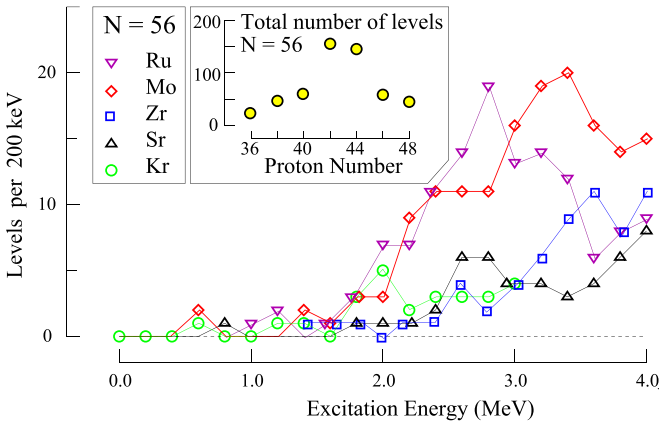

FIG. 1. Density of excited levels in $N = 56$ isotones in bins of 200 keV. The data are taken from the "Adopted Levels" of the nuclear database [13].

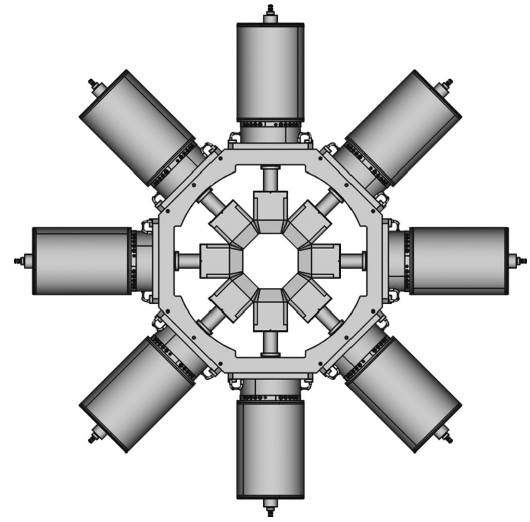

FIG. 2. γ-ray spectrometer FIPPS. Clover detectors are arranged in octagonal frame around the target position. See Refs. [19,20] for more details.

to the population of the $\nu g_{7/2}$ and $\nu h_{11/2}$ shells. Thus, the increased level density seen around 3 MeV may result from the interaction of the two higher-lying neutron shells with the $g_{9/2}$ protons. As noted in Ref. [10] configurations containing either particles or holes in the $g_{9/2}$ proton shell may also contribute to the two structures.

The population mechanism of the $\pi g_{9/2}$ shell is thus the key question in the region. Answering this question requires detailed knowledge of nuclear excitations, in particular their spins and parities. It is the purpose of this work to verify and update such spectroscopic data in neutron-rich, even-even isotones with $N = 56$. As stressed in the recent compilation of low-spin levels [16], the spin-parity assignments are of key importance.

In Sec. II we present measurements and the obtained results and compare them with previously published results, with special emphasis on spin-parity assignments. Section III provides phenomenological classifications of the results. This, confronted with the shell model calculations, helps in identifying certain excitation modes and following their development in $N = 56$ isotones. Section IV summarizes the work.

II. MEASUREMENTS AND RESULTS

A. Experiments

New experimental results on ^{92}Kr and ^{96}Zr nuclei were obtained in this work from 21-day measurements of γ rays following neutron-induced fission of ^{235}U, performed using the EXILL array of 16 large Ge detectors, including eight clover detectors in one plane with an octagonal geometry [17]. The target of ^{235}U was sandwiched between $^{\text{nat}}$Zr foils to quickly stop fission fragments. The data collected in a triggerless mode facilitated various sorting procedures. The clover detectors provided the possibility of measuring angular and directional-polarization correlations in $\gamma\gamma$ cascades. The experiments produced a significantly higher number of triple-γ coincidences, compared to the Eurogam study of ^{92}Kr [18] and ^{96}Zr [5]. A similar, detailed EXILL study of the ^{94}Sr, $N = 56$ isotone was recently reported in Ref. [12].

The EXILL campaign has shown that the combination of an intense, pencil-like neutron beam with an efficient array of germanium detectors is a powerful tool for γ spectroscopy studies. The successor of EXILL, the FIPPS array [19,20], mounted at the neutron beam of ILL, Grenoble consists of eight high-purity Ge detectors mounted in an octagonal geometry around the target position. In the present experiment a compact geometry, as shown in Fig. 2, was chosen to maximize the solid angle coverage and the coincidence efficiency. The high symmetry of the FIPPS setup allows precise angular correlations measurements and the usage of clover detectors enables linear-polarization measurements. The neutron flux at the target position reaches 10^8 cm^{-2} s^{-1}, while maintaining a small beam diameter of 15 mm [20]. The data acquisition system consists of digital electronic modules from CAEN with a sampling frequency 100 MHz.

The present work reports on the FIPPS measurement of thermal-neutron capture on a target containing 92 mg of enriched ^{97}Mo metallic powder. In the measurement, lasting 85 hours, about 5.7×10^{10} triggerless events were collected. To obtain precise energy and efficiency calibrations in a wide-energy range measurements using the standard calibration sources ^{133}Ba and ^{152}Eu as well as neutron-capture reactions ^{27}Al$(n,\gamma)^{28}$Al, ^{47}Ti$(n,\gamma)^{48}$Ti, and ^{48}Ti$(n,\gamma)^{49}$Ti were performed. To optimize the analysis of sorted histograms, constant peak-width calibration was applied, which enhances the visibility of high energy γ lines without loosing the resolving power at low γ energies. This is a second-order calibration with a large, properly adjusted quadratic term. The resulting compression of the original linear-energy spectrum, where the γ peak width (FWHM) grows proportionally to the square root of γ energy, produces γ peaks with (nearly) constant peak width over the entire spectrum.

More information on the measurements and analysis techniques can be found in Refs. [17,19–23].

TABLE I. Energies E_i and spin-parities I_i^π of excited levels in ^{92}Kr with energies E_γ and relative intensities, I_γ of their γ decays, populated in neutron-induced fission of ^{235}U, as observed in this work. Levels and decays which are new or differ from the compilation [24] are marked with an asterisk. E_f and I_f^π in the last two columns denote energies and spin-parities of levels populated by γ decays shown in column 3. New results are indicated with an asterisk.

E_i (keV)	I_i^π	E_γ (keV)	I_γ (rel.)	E_f (keV)	I_f^π
768.60(5)	2^+	768.60(5)		0.0	0^+
1446.4(2)	2^+ *	677.9(1)		768.60	2^+
		1446.1(3)		0.0	0^+
1803.5(1)	4^+	1034.90(5)		768.60	2^+
2045.7(2)	(3) *	1277.1(1)		768.60	2^+
2066.3(2)	$3^+, 4^-$*	1297.65(5)		768.60	2^+
2310.5(2) *	(4)	244.1(1) *	8(4)	2066.3	$3^+, 4^-$
		507.2(1)	100(10)	1803.5	4^+
		1541.8(2) *	36(8)	768.60	2^+
2492.0(2)	5^+ *	181.5(1)	95(9)	2310.5	(4)
		425.7(1) *	12(6)	2066.3	$3^+, 4^-$
		688.6(1)	100(12)	1803.5	4^+
2835.0(2)	(5^+) *	1031.5(1)		1803.5	4^+
2996.3(2) *	(5)	1192.8(1)		1803.5	4^+
3036.1(2)	(6^+)	969.9(2) *	26(5)	2066.3	$3^+, 4^-$
		1232.55(5)	100(9)	1803.5	4^+
3172.5(2)	(5,6) *	1106.2(1)	100(8)	2066.3	$3^+, 4^-$
		1369.0(1)	61(6)	1803.5	4^+
3178.8(2)	(5,6) *	1112.5(1)	100(5)	2066.3	$3^+, 4^-$
		1375.4(2)	18(3)	1803.5	4^+
3594.0(3)	(6,7) *	759.0(1)		2835.0	(5^+)
3627.7(2)	(7^+) *	448.8(2)	50(5)	3178.8	(5,6)
		455.4(1)	100(5)	3172.5	(5,6)
		591.6(1)	65(5)	3036.1	(6^+)
		792.8(2) *	20(4)	2835.0	(5^+)
		1136.0(2)	55(5)	2492.0	5^+
3845.9(2)	(7) *	809.8(1)	100(8)	3036.1	(6^+)
		849.8(2)	28(9)	2996.3	(5)
4123.6(3)		1288.6(1)		2835.0	(5^+)
4176.3(3)	(8) *	330.4(1)	76(5)	3845.9	(7)
		548.6(1)	100(5)	3627.7	(7^+)
4981.3(4)	(9,10) *	805.0(1)		4176.3	(8)
6339.5(5) *	(10,11,12)	1358.2(1) *		4981.3	(9,10)
6597.7(6) *	(11,12,13)	258.2(2) *		6339.5	(10,11,12)

B. Excitations in ^{92}Kr

Low-spin levels of ^{92}Kr were studied before in β^- decay of ^{92}Rb [24] while medium-spin excitations were studied in fission of ^{248}Cm [18] and ^{252}Cf [25]. In the present work we observe strong population of levels in ^{92}Kr following the neutron-induced fission of ^{235}U (some preliminary results were reported in Ref. [26]). The quality of the triple-coincidence data obtained from EXILL is illustrated in Figs. 3(a)–3(d), showing γ-ray spectra doubly gated on lines of ^{92}Kr. The spectra are discussed in the text below.

The present work confirms most of the levels listed in the compilation [24] and adds four new levels and seven new transitions to the level scheme of ^{92}Kr. Table I lists levels and transitions of ^{92}Kr observed in this work. Only those transitions and decay branchings which are observed in coincidence spectra are shown. New results obtained in this work are marked in Table I with asterisks.

Figure 4 shows a partial scheme of excited levels in ^{92}Kr obtained in this work. To assist further discussion we show at the left-hand side of the figure all low-spin levels below 4 MeV (without decays) populated in β^- decay [24], which are not seen in the present work.

The present work does not confirm the 358-keV decay of the 1803.5-keV level, reported in [24]. The order of transitions in the 181.5–507.2-keV cascade is reversed compared to [24] because of the new, 1541.8-keV decay to the 768.60-keV level. In Fig. 3(a) we show a γ spectrum doubly gated on the 768.6- and 181.5-keV lines where the 1541.8-keV line is clearly seen. Therefore the 1985.2-keV level, reported previously [24], does not exist, and instead we introduced a new level at 2310.5 keV. The new order is supported by the weak, 244.1-keV decay from the 2310.5-keV level. The 1297.7-keV peak is too weak to be seen in this spectrum, but is clearly seen in a spectrum doubly gated on the 768.6- and 244.1-keV lines, shown in Fig. 3(b).

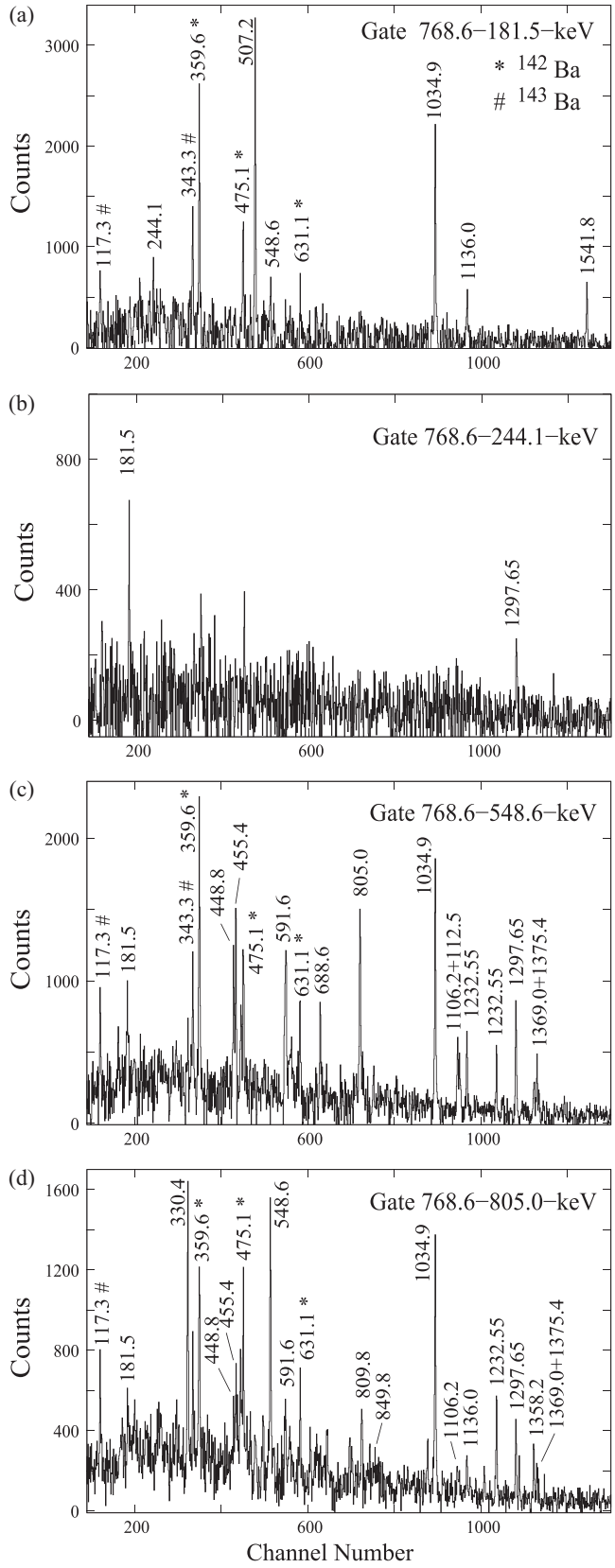

FIG. 3. Coincidence γ spectra doubly gated on lines of ^{92}Kr, as observed in the present work, following neutron-induced fission of ^{235}U. Lines belonging to the ^{142}Ba and ^{143}Ba, complementary fission fragments [27–29] are marked with symbols * and #, respectively.

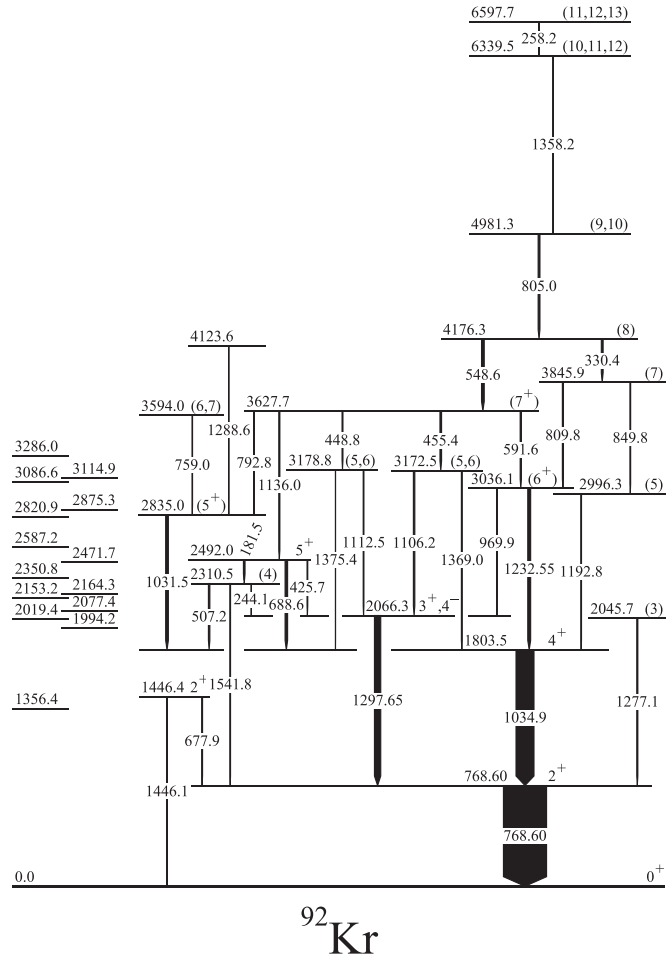

FIG. 4. Partial level scheme of ^{92}Kr as obtained in this work from fission of ^{235}U induced by thermal neutrons. The widths of arrows are proportional to the observed γ intensity. Levels without decays are drawn on the left-hand side after Ref. [24] to help further discussions.

The order of the 1192.8- and 849.8-keV transitions in the cascade depopulating the 3845.9-keV level is reversed compared to Ref. [24] because of higher intensity of the 1192.8-keV line seen in the respective coincidence spectra. In the spectrum doubly gated on the 768.6- and 1192.8-keV lines the number of counts in the 1034.9-keV line is 1650(115) whereas in the 849.8-keV line it is 830(95), only. If the 849.8-keV transition was below the 1192.8-keV one, counts in the 1034.9- and 830(95)-keV lines should be equal. Consequently, we introduce a new level at 2996.3 keV, instead of the 2653.3-keV level reported previously [24].

The 1358.2-keV transition (1358.3-keV in Ref. [25]), seen in Fig. 3(d) feeds the 4981.3-keV level and defines a new level at 6339.5 keV. In a spectrum gated on the 768.6- and 1358.2-keV lines there is a new line at 258.2 keV. A spectrum gated on the 258.2- and 768.6-keV lines shows the 1358.2-keV line and other lines belonging to ^{92}Kr. Therefore, we propose a new level at 6597.7 keV.

We do not confirm the 2684.0-, 2698.9-, 4185.4-, and 4394.9-keV levels reported in Ref. [25]. The 32.5-keV link

TABLE II. Angular correlation coefficients for γ-γ cascades in ^{92}Kr populated in neutron-induced fission of ^{235}U. The label "sum" denotes summed correlations with all quadrupole transitions below the $E_{\gamma 1}$.

$E_{\gamma 1}$-$E_{\gamma 2}$ cascade	A_2/A_0 exp.	A_4/A_0 exp.	Spins in cascade	$\delta_{\rm exp}(\gamma 1)$
677.9–768.60	0.103(40)	0.150(92)	2-2-0	0.25(5)
				or −4.1(9)
1034.9–768.60	0.108(11)	−0.041(26)	4-2-0	
1277.1–768.60	−0.06(12)	0.04(28)	Not 4-2-0	
1297.65–768.60	0.106(18)	−0.042(40)	3-2-0	2.3(2)
				or 0.25(3)
			4-2-0	
688.6-1034.9	−0.41(6)	0.10(9)	5-4-2	−1.0(5)
1031.5-1034.9	0.052(25)	0.034(60)	4-4-2	0.40(7)
			5-4-2	0.17(4)
1232.55-sum	0.102(22)	0.037(49)	5-4-2	0.28(5)
			6-4-2	

between the 3627.7- and 3594.0-keV levels, suggested in Ref. [18], is not confirmed.

The summed intensity of all γ transitions feeding the 2_1^+ level at 768.60 keV in ^{92}Kr yields only about 70% of the intensity of the 768.60-keV line, as seen in the γ spectrum doubly gated on the 359.6- and 475.1-keV lines of the ^{142}Ba complementary fission fragment. This suggest a significant, unknown feeding to the 2_1^+, 768.60-keV level in ^{92}Kr. The missing intensity could not be identified in the present work. We note that the 769-keV peak in the γ spectrum from fission of ^{235}U $+n$ is rather complex and needs more attention. An analogous puzzle concerning the population of ^{91}Kr was recently resolved by careful analysis of the 707-keV multiplet [30].

Spins and parities of levels in ^{92}Kr were proposed based on angular and directional-polarization correlations measured in this work and shown in Tables II and III, respectively. We also used the yrast-population argument [31] and the fact that in this work no delayed decays in ^{92}Kr with half-lives longer than 10 ns were observed.

Spin $I = 1$ of the 1446.4-keV level reported in [24] is excluded by angular correlations and we assign spin-parity 2^+ to this level. Spin-parity 2^- or 3^- is less likely due to the large mixing ratio, δ, of the 677.9-keV transition and the strong 1446.1-keV decay to the ground state.

Spin $I = 4$ is confirmed for the 1803.5-keV level but the linear polarization could not be determined due to the tight doublet of 1031.5- and 1034.9-keV lines. We adopt positive parity in agreement with the compilation [24].

Angular correlations for the 1277.1–768.60-keV cascade suggest spin $I < 4$ for the 2045.7-keV level (this level is also reported in β^- decay). Spin $I = 3$ is favored over $I = 2$ because of the direct population of this level in fission, which preferentially populates yrast states.

An interesting result is obtained for the 2066.3-keV level, reported with firm $I = 4$ spin in Ref. [24]. Our angular correlations allow both $I = 3$ and $I = 4$. However, the negative sign of the linear polarization obtained for the 1297.65-keV transition favors spin-parity 3^+ or 4^-. The latter is less likely in view of the strong, prompt decay to the 2_1^+ level.

Angular correlations for the 688.6–1034.9-keV cascade provide only one solution, $I = 5$ for the spin of the 2492.0-keV level. The large $\delta = -1.0(5)$ favors positive parity for this level.

Angular correlations for the 1031.5–1034.5-keV cascade provide two solutions for spin of the 2835.0-keV level, $I = 4$ or $I = 5$. A tentative, (5^+) spin-parity assignment to this level is preferred because of the 792.8-keV feeding from the (7^+) level at 3627.7 keV and the obtained δ value.

Angular correlations for the 1232.55-keV transition in cascade with the sum of 678.60- and 1034.9-keV transitions provide $I = 5$ or $I = 6$ solution for the 3036.1-keV level. High intensity of the prompt, 1232.55-keV transition suggests yrast character and spin-parity $I = (6^+)$ of this level.

Other tentative spin assignments shown in Fig. 4 were proposed based on the observed decay branching and the yrast-population argument [31].

TABLE III. Experimental, $P_{\rm exp}(\gamma_1)$ and theoretical, $P_{\rm th}(\gamma_1)$ values of linear polarization for the γ_1 (upper) transition in a γ_1-γ_2 cascade of ^{92}Kr, as obtained from directional-polarization correlations in this work. The correlating 768.60-keV γ_2 is a $\Delta I = 2$, stretched $E2$ transition with $\delta = 0$.

$E_{\gamma 1}$-$E_{\gamma 2}$	$P_{\rm exp}(\gamma 1)$	Spin-parity	$\delta_{\rm exp}(\gamma 1)$	$P_{\rm th}(\gamma 1)$
1232.55–768.60	+0.26(29)	5^+-4^+-2^+	0.28(5)	−0.215(20)
		6^+-4^+-2^+	0.0	+0.167
1297.65–768.60	−0.25(20)	3^+-2^+-0^+	0.25(3)	−0.226(16)
			2.3(2)	−0.499(8)
		4^+-2^+-0^+	0.0	+0.167
		4^--2^+-0^+	0.0	−0.167

In our data there is a very small, if any, population due to β^- decay of ^{92}Br and we do not observe non-yrast levels shown (without decays) to the left of Fig. 4. Some of these levels are reported with spin 1 or 2^+ [24], which may suggest low spin of the β-decaying state, but there is also a clear population of the 4^+ level at 1803.5 keV in ^{92}Kr in β^- decay of ^{92}Br [24]. In Ref. [32] a tentative spin-parity (3^-) was proposed for the ground state of ^{92}Br. However, spin $I = 3$ is not consistent with the very small overlap between β-decay and prompt-γ excitation schemes of ^{92}Kr. In the present work we do observe the 2045.7-keV level seen in β decay but the 2066.3-keV level with a likely spin $I^\pi = 3^+$ is not seen in β decay [24]. This suggests either a low spin of the ground state in ^{92}Br or a special collective nature of the 2066.3-keV level.

We do not observe the 1356.4 keV level reported in [24] with $\log ft > 7.4$. This level should have spin $I = 0$ or $I = 1$, considering the yrast-population argument [31]. It is of high interest to verify this information.

C. Excitations in ^{96}Zr

Numerous studies of ^{96}Zr, reviewed in the compilation [33], provided detailed data on low-spin levels, obtained from transfer, β-decay, and $(n, n'\gamma)$ measurements. Less is known about medium spin levels. The medium-spin part of the level scheme is expected to provide key information on the development of collective structures in ^{96}Zr. The heavy-ion-induced-fission study [34] provided some tentative spin-parity assignments but this important information has not been verified to date in any other measurement of ^{96}Zr fission fragments. One of the reasons may be the rather weak population of ^{96}Zr in spontaneous fission of ^{248}Cm or ^{252}Cf. Recent measurement of γ rays following cold-neutron-induced fission of ^{235}U [17], performed at ILL Grenoble using EXILL, provided high-statistics data on ^{96}Zr and the means to determine spins and parities from angular and directional-polarization correlations [22]. In the following we verify the existing data and report new information on ^{96}Zr, based on the EXILL measurement.

In the EXILL data there is a visible population of levels in ^{96}Zr in the neutron-induced fission and a very strong population in β^- decay of the 0^- ground state and the 8^+ isomer in ^{96}Y, a secondary fission fragment located near the maximum of the production in fission of ^{235}U. The quality of triple-coincidence data obtained from EXILL is illustrated in Fig. 5, which shows examples of γ spectra doubly gated on lines of ^{96}Zr. The spectra are discussed in the text below.

Excited levels in ^{96}Zr observed in this work are listed in Table IV and shown in Fig. 6. Only those transitions and decay branchings which are observed in doubly gated coincidence spectra are shown in Table IV. In several cases decay branchings observed in the doublygated spectra differ from those reported in Ref. [33]. To assist further discussions we show to the right of Fig. 6 other low-spin levels (without their decays) reported in Ref. [33] below 4 MeV of excitation, which are not observed in this work.

Spin-parity assignments to levels in ^{96}Zr shown in Fig. 6 and Table IV are based on angular and directional-polarization correlations measured in this work and listed in Tables V and VI, respectively, and on decay branchings.

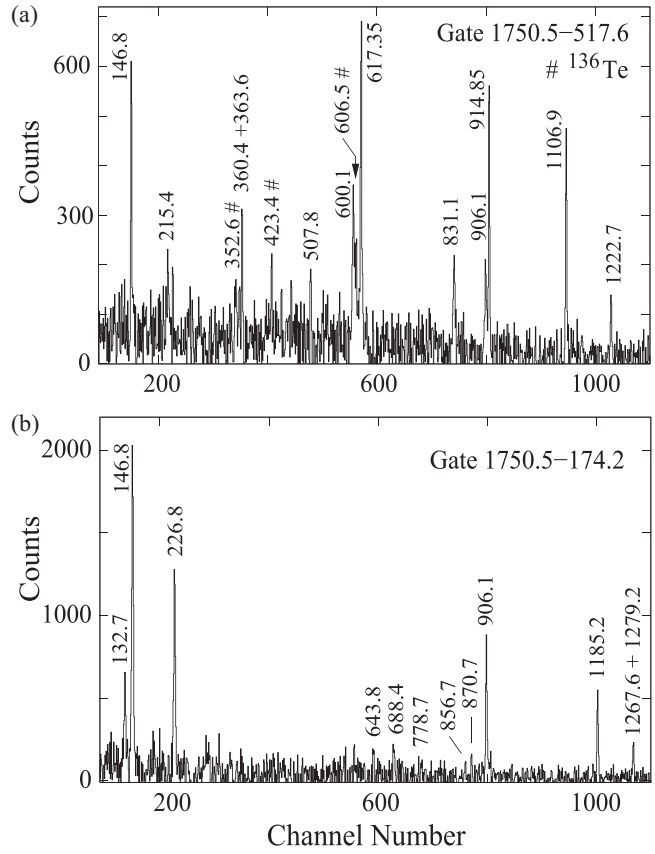

FIG. 5. Coincidence γ spectra doubly gated on lines of ^{96}Zr, as observed in the present work, following neutron-induced fission of ^{235}U. Lines belonging to the ^{136}Te complementary fission fragment [35] are marked with the "#" symbol.

The present work confirms most of the levels and transitions listed in the compilation [33]. New or significantly different results, as compared to Ref. [33], are marked in Table I with asterisks. All the data shown in Tables V and VI are new.

In the present measurement the precision on γ energies was limited to 0.05 keV. The decays of low-energy excited levels reported in the compilation [33] have better precision. However, at higher excitations the present work gives more accurate energies [for example, for the 4389.5(5)-keV level reported in [33] the present work gives an energy of 4389.60(10) keV].

Our angular and directional-polarization data confirm spin-parity assignments in the ground-state cascade up to the 8^+, 4389.60-keV level. However for the 4907.2-keV level we propose tentative spin-parity (9^+) instead of (10^+) proposed in Ref. [34]. This is based on our angular correlations, consistent with spin-parity $I = 8$ or $I = 9^+$. The strong population of this level in heavy-ion-induced fission [34], populating predominantly yrast levels, and its weak population in β decay [33] favor the $I = 9$ solution.

The 5507.1-keV level with $\log ft = 5.2$ is probably populated by the $\nu g_{7/2} \rightarrow \pi g_{9/2}$, Gamow-Teller transition from the 8^+ isomer in ^{96}Y at 1140 keV [33]. Spin-parity 8^+ for the 5507.1-keV level is the most likely solution considering its

TABLE IV. Experimental properties of excited levels in ^{96}Zr observed in neutron-induced fission of ^{235}U. New results are indicated with an asterisk.

E_i (keV)	I_i^π	E_γ (keV)	I_γ (rel.)	E_f (keV)	I_f^π
1750.50(5)	2^+	1750.50(5)		0.0	0^+
1897.30(5)	3^-	146.80(5)	100(3)	1750.50	2^+
		1897.30(5)	16(1)	0.0	0^+
2225.85(5)	$2^{(+)}$	328.6(1)	8(2)	1897.30	3^-
		475.40(5)	90(5) *	1750.50	2^+
		644.2(1)	26(2)	1581.65	0^+
		2225.80(5)	100(4)	0.0	0^+
2438.8(2)	3^+	688.4(2)		1750.50	2^+
2857.40(5)	4^+	631.60(5)	16(1)	2225.85	2^+
		960.10(5)	8(1)	1897.30	3^-
		1106.90(5)	100(3)	1750.50	2^+
3082.50(10)	4^+	643.8(3)	8(3)	2438.8	3^+
		856.7(3)	9(3)	2225.85	2^+
		1185.20(5)	100(7)	1897.30	3^-
3120.00(10)	5^-	1222.70(5)		1897.30	3^-
3176.5(2)	4^+	1279.2(1)		1897.30	3^-
3309.3(1)	(5^+)	132.7(1)	47(5)	3176.5	4^+
		189.4(2)	7(3)	3120.00	5^-
		226.8(1)	100(6)	3082.50	4^+
		870.7(3) *	10(5)	2438.8	3^+
3483.55(15)	6^+	174.2(1)	7(1)	3309.3	(5^+)
		363.60(5)	100(3)	3120.00	5^-
		401.4(4)	1.0(5)	3082.50	4^+
		626.1(1)	4(1)	2857.40	4^+
3772.20(10)	6^+	289.0(2)	1.5(2)	3483.55	6^+
		652.15(15)	2.5(4)	3120.00	5^-
		689.7(2)	2.4(4)	3082.50	4^+
		914.85(5)	100(3)	2857.40	4^+
4126.5(2)	(6,7) *	1006.0(1)		3120.00	5^-
4234.5(2)	7^-	750.8(2)	20(10)	3483.55	6^+
		1114.6(1)	100(12)	3120.00	5^-
4262.3(3)	(6^+) *	490.1(1)	100(20)	3772.20	6^+
		778.7(2)	90(20)	3483.55	6^+
		1085.6(3) *	20(10)	3176.5	4^+
		1180.3(3)	30(15)	3082.50	4^+
4389.60(10)	8^+	155.2(2)	0.5(2)	4234.5	7^-
		617.35(5)	100(6)	3772.20	6^+
		906.10(5)	25(5)	3483.55	6^+
4690.3(4)	(8) *	455.8(2)		4234.5	7^-
4751.3(2)	$(7,8)^+$ *	979.1(1)	100(10)	3772.20	6^+
		1267.6(3) *	70(15)	3483.55	6^+
4846.2(3)	(7,8,9) *	719.7(1)		4126.5	(6,7)
4907.2(2)	(9^+) *	517.6(1)		4389.60	8^+
5066.7(3)	$(7^+, 8^+)$	315.3(3)	32(4)	4751.3	$(7, 8^+)$
		804.5(2)	100(10)	4262.3	(6^+)
		1583.1(1)	95(5)	3483.55	6^+
5484.3(3)	(10^+)	1094.7(2)		4389.60	8^+
5507.1(2)	(8^+) *	600.1(2)	45(5)	4907.2	(9^+)
		755.7(2)	14(2) *	4751.3	$(7, 8^+)$
		1117.5(1)	100(3)	4389.60	8^+
		1272.7(2) *	28(3)	4234.5	7^-
		1735.0(2)	15(3)	3772.2	6^+
5738.3(3)	(11^+)	831.1(1)	100(15)	4907.2	(9^+)
		254.4(4) *	20(8)	5484.3	(10^+)
6246.1(4)	(12^+)	507.8(1)		5738.3	(11^+)
6461.5(5)	(13^+)	215.4(3)		6246.1	(12^+)
6821.9(7)	(14^+)	360.4(4)		6461.5	(13^+)

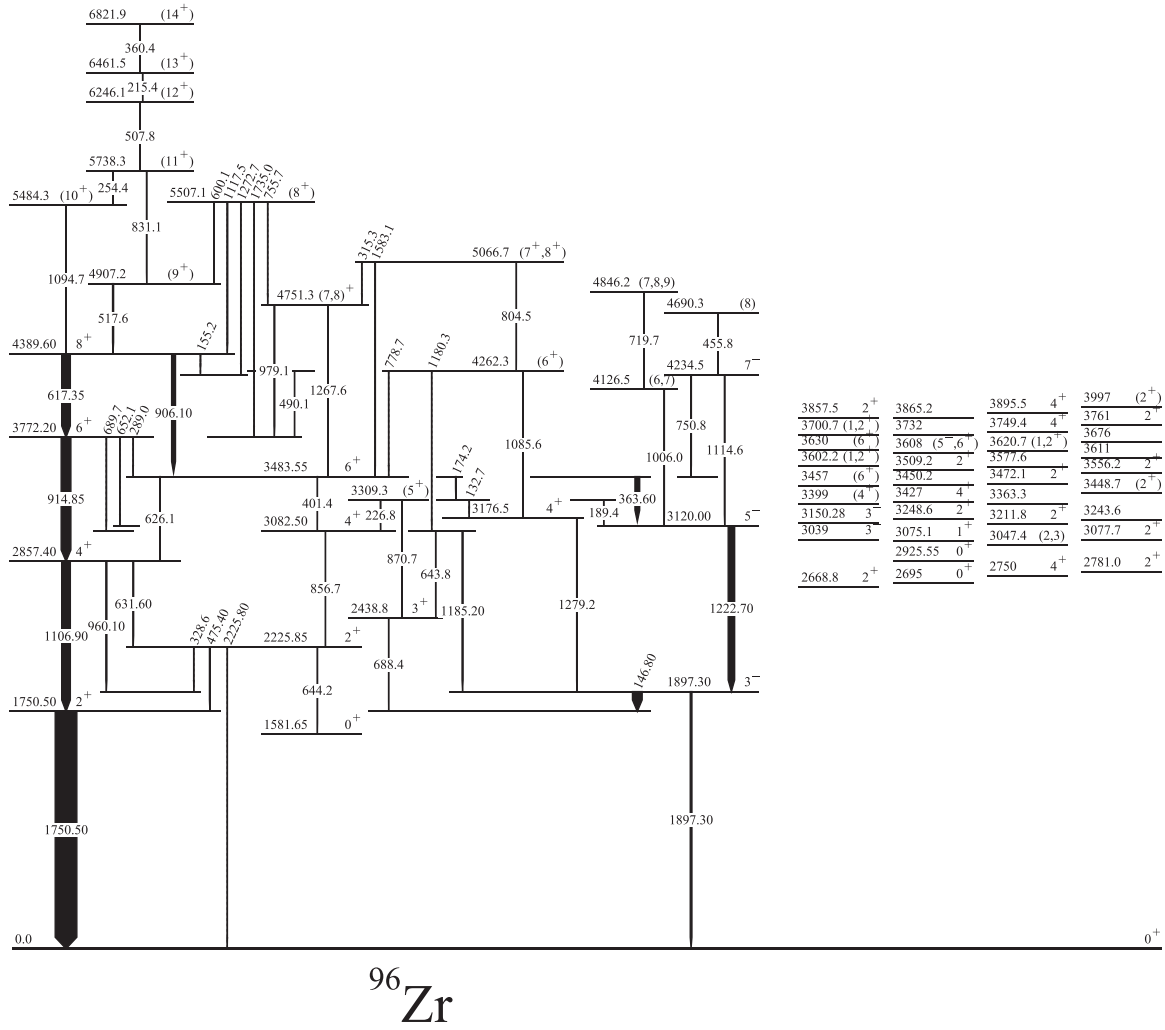

FIG. 6. Partial level scheme of ^{96}Zr obtained in this work in measurements of γ rays from the neutron-induced fission of ^{235}U. At the right-hand side all levels (without decays) which are reported in Ref. [33] and not observed in the present work are shown to assist further discussions.

non-yrast character; it is not reported in Ref. [34] and has the 1272.7-keV decay to the (6^+) level, introduced in this work.

Higher-spin levels in the ground-state cascade are observed in the present work with low intensities. This suggests their population in prompt-γ fission, only. Unlike levels with lower spins, which may be populated in β^- decay of ^{96}Y, the levels with spins higher than $I = 10$ are not populated in β decay of the 8^+ isomer in ^{96}Y. The yrast-population argument suggests their spins grow with energy, and we adopt spins reported in Ref. [34]. The new, 254.4-keV decay from the 5738.3-keV level is consistent with these spins.

Our angular correlations are consistent with the 3^- and 5^- spin-parity values of the 1897.30- and 3120.00-keV levels, respectively, though no linear polarization is available for the 146.80- and 363.60-keV dipole transitions. A dipole character for the 1185.2-keV transitions is suggested by angular correlation coefficients in the 1185.20–1750.50-keV cascade. We note that the unobserved 146.80-keV intermediate transition of a stretched dipole character does not change the correlation; it is marked (-u-) in Table V.

Finally, we comment on some of the levels shown to the right of Fig. 6. It is unlikely that the 2750-keV level has spin-parity 4^+, as reported in the compilation [33]. With such a spin-parity this level would be yrast and visibly populated following fission, which is not the case. A similar comment concerns the 3457- and 3630-keV levels reported with spin-parity (6^+) [33]. These levels, proposed in transfer-reaction studies, were not reported in any measurement of γ decays in ^{96}Zr.

The systematics of 0^+ excited states shown in Figs. 5 and 6 of Ref. [10] suggested that there may be an extra 0^+ level around 1.0 MeV in ^{96}Zr. In the present work we could not see such a level. However, levels at 1581.65, 2225.85, 2438.8, 3082.50, 3176.5, 3309.3, 3483.55, 4262.3, 4751.3, and 5066.7 keV, shown in the middle of Fig. 6, can be arranged into "bands," starting form the 0^+ level at 1581.65 keV, because of the linking transitions, including new, 870.7-, 1085.6- and 1267.6-keV decays. The new 870.7-keV decay of the 3309.3-keV level and the lack of decays to 2^+ levels favor spin-parity 5^+ for this level. The large mixing ratio, $\delta = 0.36(5)$, of the 979.1-keV decay of the 4751.3-keV

TABLE V. Angular correlation coefficients for γ-γ cascades in ^{96}Zr populated in neutron-induced fission of ^{235}U. Label "sum" denotes summed correlations with all stretched transitions below the $E_{\gamma 1}$.

$E_{\gamma 1}$-$E_{\gamma 2}$ cascade	A_2/A_0 exp.	A_4/A_0 exp.	Spins in cascade	$\delta_{\rm exp}(E_{\gamma 1})$
146.80–1750.50	−0.069(8)	−0.030(18)	3-2-0	0.003(10)
363.60–1222.70	−0.66(12)	−0.054(24)	6-5-3	0.001(12)
475.40–1750.50	0.44(8)	−0.43(22)	2-2-0	0.29(15)
517.6–sum	0.212(70)	−0.19(16)	8-8-6	−0.16(40)
			9-8-6	1.4(9)
617.35–sum	0.100(10)	−0.027(21)	8-6-4	
914.85–sum	0.095(9)	0.015(19)	6-4-2	
979.1–sum	0.130(19)	0.004(42)	7-6-4	0.36(5)
			8-6-4	
1106.9–1750.50	0.106(10)	−0.007(21)	4-2-0	
1117.5–sum	0.141(48)	−0.09(11)	8-8-6	2.2(7)
			9-8-6	0.41(15)
			Spins in cascade	
1185.2–1750.50	−0.052(65)	−0.19(14)	4-3 (-u-) 2-0	
1222.70–1750.50	0.105(12)	−0.18(14)	5-3 (-u-) 2-0	

level and its new, 1276.6-keV decay favor positive parity for this level. Further comments on possible band structurs in ^{96}Zr are given in Sec. III C.

D. Excitations in ^{98}Mo

The ^{98}Mo nucleus has been the subject of many experimental works, listed in the recent compilation [36]. We note the high- and medium-spin studies [37–39] and the previous ^{97}Mo$(n_{\rm th}, \gamma)^{98}$Mo measurement [40], the latter done five decades ago. Low-spin levels of ^{98}Mo were also studied in β^- decay of the 1^+ ground state [41,42] and the (5^+) isomer of ^{98}Nb [43]. Note also the recent total absorption spectrometry near β stability, improving our knowledge not only about reactor-based physics but also about the low-energy 0^+ excitations and the β-decay process in the region [44–46].

The present measurement of thermal-neutron capture on a ^{97}Mo target performed using the FIPPS array provided significantly more data as compared to the work [40], and was primarily concentrated on the verification of known and determination of new spin-parity assignments to levels in ^{98}Mo via precise angular correlations (of quality comparable to those in Ref. [39]) and linear-polarization correlations reported here for the first time.

In our measurement over 600 γ transitions, depopulating over 200 excited levels, were identified in ^{98}Mo. This includes 129 primary γ transitions from the neutron capture level. The presentation and the discussion of this full data set is beyond the scope of the present work and will be published elsewhere [23]; below we show partial results obtained in this work, which are relevant to the present discussion of $N = 56$ isotones.

Our data are shown in the level scheme in Fig. 7 and listed in Tables VII, VIII, and IX. In Table VII we list all levels up to 3.3 MeV with all their γ decays, as seen in this work. Intensities of all γ decays in Table VII are in the same relative units with the intensity of the 778.15-keV decay line normalized to 1000. The summation effect in the present data in $\gamma\gamma$ cascades is lower than 0.0022. Therefore, none of the reported ground-state transitions is a sum peak. New levels and decays or those which differ significantly from the compiled values [36] are marked with an asterisk. All results shown in Table IX are new. The correlating γ_2 transitions in these tables are of stretched character.

As the ground state of ^{97}Mo has spin-parity $5/2^+$, one can expect population of excited levels with spins up to $I = 6$ following the ^{97}Mo$(n_{\rm th}, \gamma)^{98}$Mo reaction. Indeed, five $I^\pi = 6^+$ levels are reported in the present scheme of ^{98}Mo: three levels at 2343.72, 2678.79, and 2836.89 keV reported with spin-parity 6^+ [36] and the 3021.51- and 3211.58-keV levels, reported in [36] with spin-parity 4^+.

Because the neutron-capture reaction is considered to be a tool for a "complete spectroscopy," populating all levels with spins up to the limit (here $I = 6$), the observation or nonobservation of levels in ^{98}Mo in the ^{97}Mo$(n_{\rm th}, \gamma)^{98}$Mo reaction puts limits on their spins. In this respect it is useful to compare the present data to those of the medium-spin studies [37–39].

In the present work we do not see any level with spin $I = 7$ reported in [36]. This indicates that the 2570.9-keV level reported with spin (6,7,8) [36] probably has spin higher than $6\hbar$. The 2739-keV level reported with tentative spin $I = (6, 7)$ [37] has spin $I = 7$ and confirms spin $I = 7$ for the the 3097-keV level [36,37] (surprisingly, the 2739-keV level is not reported in the $(\alpha, 2n)$ reaction [39]). The 2853.71-keV level reported in [39] with tentative spin ranging from 5 to 8 is not seen in our data, which suggests its spin higher than 6, in accord with the (8^+) assignment in [37]. Analogously, the 3271.24-keV level reported in [39] with a tentative spin ranging from 6 to 8 should have spin higher than 6 because it is not seen in our data. In the high-spin work [37] this level was reported in the ground-state band with spin (8^+). The 3228.71-keV level reported in [39] with tentative spin ranging from 5 to 8, which is not seen in our work, might have spin higher than 6 but in the compilation [36] this level (3229.17 in [36]) is reported with spin-parity (4^+). This level is not seen in the high-spin work [37], adding to the inconsistency. Finally, we note that the 2644.7-keV level, reported with spin $(1, 2^+)$ is not seen in our data; the intensity of the (unobserved) 1212.7-keV decay from this level to the 1432.28-keV level

TABLE VI. Experimental values, $P_{\rm exp}(\gamma_1)$, of linear polarization for the γ_1 (upper) transition in a γ_1-γ_2 cascade of ^{96}Zr, populated in neutron-induced fission of ^{235}U, as obtained from directional-polarization correlations in this work. The correlating γ_2 line of 1750.50 keV is assumed to be a stretched, $E2$ transition with $\delta = 0$ and theoretical $P_{\rm th}(\gamma_1)$. The theoretical value of the directional-polarization correlation in a cascade of two stretched, unmixed $E2$ transitions is $P_{\rm th}(\gamma) = 0.1667$.

$E_{\gamma 1}$-$E_{\gamma 2}$	$P_{\rm exp}(\gamma 1)$
617.35–1750.50	0.15(3)
914.85–1750.50	0.19(4)
1106.90–1750.50	0.18(4)

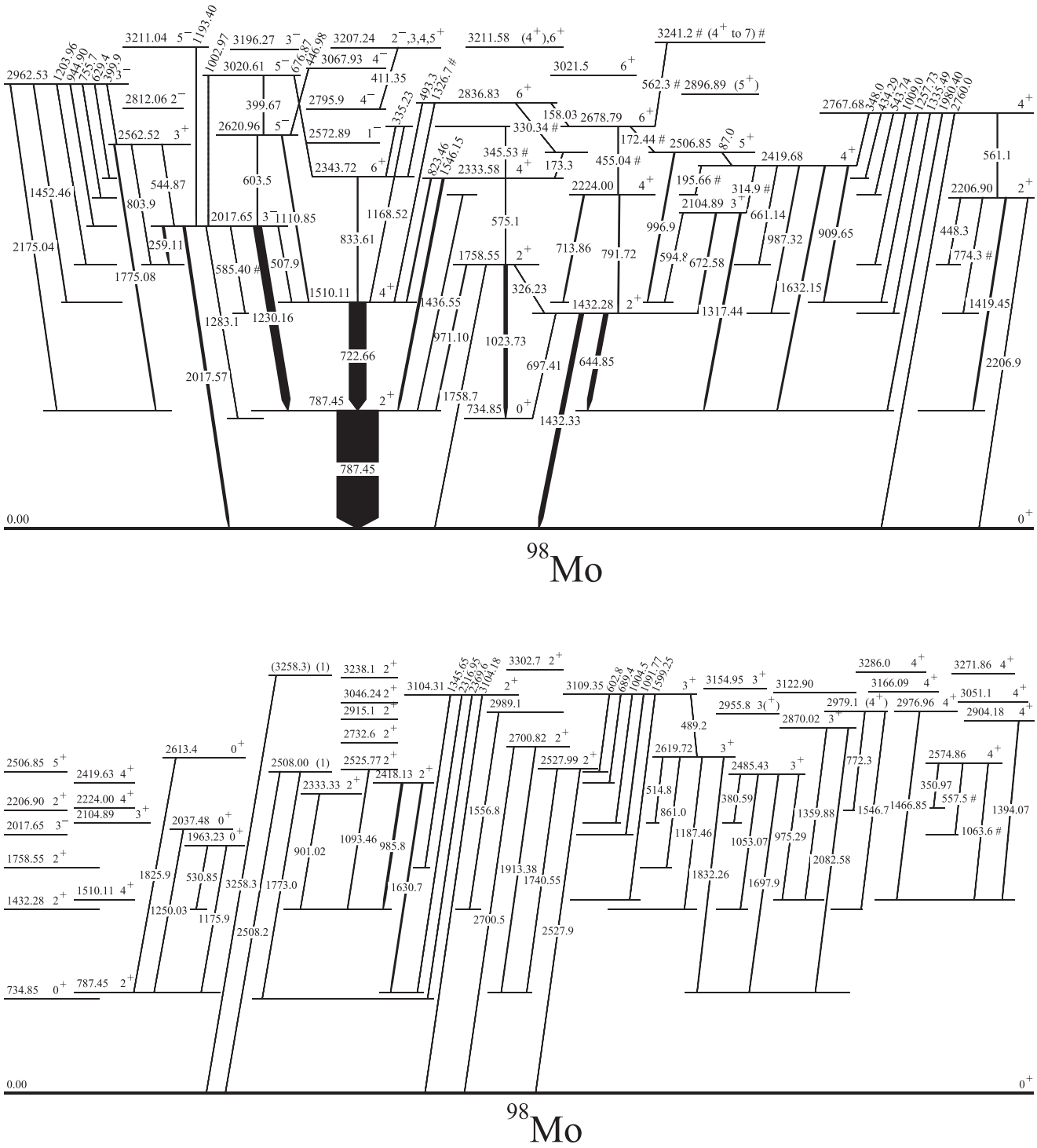

FIG. 7. Partial level scheme of ^{98}Mo obtained in this work from measurements of γ rays following thermal-neutron capture on the ^{97}Mo target. Thickness of a γ line is proportional to its intensity observed in the present work. For some high-energy, non-yrast levels their decays are not shown. See Table VII for these decays. Symbol # denotes data taken from Ref. [36].

is lower than 2% of the intensity of the 791.72-keV transition feeding the 1432.28-keV level.

Spins of levels were determined previously based on various reaction data [36] and, most notably, on precise angular correlations reported in Ref. [39]. Based on nonzero values of δ mixing ratio of γ decays as well as half-lives of levels, parities for these levels were proposed.

The present angular correlations, shown in Table VIII are of comparable accuracy to those of Ref. [39]. However, the linear-polarization correlations, shown in Table IX, besides providing an experimental information on parities of levels,

TABLE VII. Experimental properties of excited levels in ^{98}Mo populated in thermal-neutron capture reaction. New results are indicated with an asterisk.

E_i (keV)	I_i^π	E_γ (keV)	I_γ (rel.)	E_f (keV)	I_f^π
734.85(8)	0^+				
787.45(3)	2^+	787.45(3)	1000(57)	0.00	0^+
1432.28(2)	2^+	644.85(3)	102(6)	787.45	2^+
		697.41(4)	5.3(3)	734.85	0^+
		1432.33(5)	97(6)	0.00	0^+
1510.11(3)	4^+	722.66(3)	339(19)	787.45	2^+
1758.55(3)	2^+	326.23(5)	3.6(2)	1432.28	2^+
		971.10(4)	49.3(9)	787.45	2^+
		1023.73(5)	77(4)	734.85	0^+
		1758.7(1)	7.9(5)	0.00	0^+
1963.23(6)	0^+	530.85(8)	0.9(1)	1432.28	2^+
		1175.9(1)	2.2(1)	787.45	2^+
2017.65(1)	3^-	259.11(2)	45(2)	1758.55	2^+
		507.9(2)	10.1(6)	1510.11	4^+
		1230.16(3)	191(11)	787.45	2^+
		1283.1(3)	0.7(1)	734.85	0^+
		2017.57(3)	50(3)	0.00	0^+
2037.48(5)	0^+	1250.03(5)	3.9(2)	787.45	2^+
2104.89(3)	3^+	594.8(1)	5.1(3)	1510.11	4^+
		672.58(3)	24(1)	1432.28	2^+
		1317.44(8)	36(2)	787.45	2^+
2206.90(4)	2^+	448.3(2)	1.4(1)	1758.55	2^+
		1419.45(4)	30(2)	787.45	2^+
		2206.9(1)	1.1(1)	0.00	0^+
2224.00(4)	4^+	713.86(7)	25(1)	1510.11	4^+
		791.72(6)	20(1)	1432.28	2^+
		1436.55(8)	9.5(6)	787.45	2^+
2333.33(3)	2^+	901.02(3)	6.2(4)	1432.28	2^+
2333.58(3)	4^+	575.1(2)	2.8(2)	1758.55	2^+
		823.46(4)	19(1)	1510.11	4^+
		1546.15(5)	45(3)	787.45	2^+
2343.72(2)	6^+	833.61(2)	13.0(7)	1510.11	4^+
2418.13(7)	2^+	985.8(1)	39(2)	1432.28	2^+
		1630.7(1)	23(1)	787.45	2^+
2419.68(2)	4^+	402.1(1)	1.7(1)	2017.65	3^-
		661.14(6)	3.4(2)	1758.55	2^+
		909.65(4)	17.2(9)	1510.11	4^+
		987.32(5)	15.6(9)	1432.28	2^+
		1632.15(4)	22(1)	787.45	2^+
2485.43(3)	3^+	380.59(4)	2.4(1)	2104.89	3^+
		975.29(6)	4.5(3)	1510.11	4^+
		1053.07(6)	5.7(3)	1432.28	2^+
		1697.9(1)	11.7(7)	787.45	2^+
2506.9(1)	5^+	87.0(2)	0.3(1)	2419.68	4^+
		173.3(2)	3.0(2)	2333.58	4^+
		996.9(2)	7.4(4)	1510.11	4^+
2508.00(7)	(1)	1773.0(1)*	0.7(1)	734.85	0^+
		2508.2(1)*	0.8(1)	0.00	0^+
2525.77(3)	2^+	1093.46(3)	10.3(6)	1432.28	2^+
2527.99(7)*	2^+	1740.55(7)*	2.2(1)	787.45	2^+
		2527.9(2)*	0.2(1)	0.00	0^+
2562.52(3)	3^+ *	544.87(6)	1.6(1)	2017.65	3^-
		803.9(1)	1.3(1)	1758.55	2^+
		1775.08(4)	27(2)	787.45	2^+
2572.89(3)	1^-	239.72(7)	1.1(1)	2333.33	2^+
		555.1(4)	8.9(5)	2017.65	3^-
		814.34(6)	9.1(5)	1758.55	2^+
		1140.56(7)	3.6(2)	1432.28	2^+
		1785.39(4)	14.9(9)	787.45	2^+
		2572.5(5)*	0.6(1)	0.00	0^+
2574.97(3)	4^+	350.97(3)	6.9(4)	2224.00	4^+
2613.4(3)	0^+	1825.9(3)	0.92(6)	787.45	2^+
2619.72(3)	3^+	514.8(1)*	1.20(7)	2104.89	3^+
		861.0(1)*	3.6(2)	1758.55	2^+
		1187.46(4)	4.9(3)	1432.28	2^+
		1832.26(4)	11.0(6)	787.45	2^+
2620.96(7)	5^-	603.5(1)	8.4(5)	2017.65	3^-
		1110.85(5)	16.8(10)	1510.11	4^+
2678.79(3)	6^+	335.23(4)	0.30(2)	2343.72	6^+
		1168.52(4)	2.1(1)	1510.11	4^+
2700.82(4)	2^+	1913.38(4)	10.6(6)	787.45	2^+
		2700.5(3)*	1.8(1)	0.00	0^+
2732.6(1)	2^+	1945.1(1)	10.9(6)	787.45	2^+
2767.68(2)	4^+	348.0(1)	0.85(5)	2419.68	4^+
		434.29(5)	2.6(1)	2333.58	4^+
		543.74(6)	1.61(9)	2224.00	4^+
		561.1(1)	0.54(3)	2206.90	2^+
		1009.0(2)	0.33(2)	1758.55	2^+
		1257.73(5)	2.5(1)	1510.11	4^+
		1335.49(6)	3.2(2)	1432.28	2^+
		1980.40(3)	8.8(5)	787.45	2^+
		2767.0(3)*	0.22(2)	0.00	0^+
2795.9(3)	4^-	1285.8(3)	28(2)	1510.11	4^+
2812.06(4)	2^-*	2024.61(4)	7.3(4)	787.45	2^+
2836.89(6)	6^+	158.03(7)	0.91(7)	2678.79	6^+
		493.3(1)	0.07(1)	2343.72	6^+
2870.02(2)	3^+*	1359.88(4)*	2.6(1)	1510.11	4^+
		2082.58(3)	7.6(5)	787.45	2^+
2896.89(7)	(5^+)	792.0(1)	3.8(2)	2104.89	3^+
		1386.8(1)	3.4(2)	1510.11	4^+
2904.18(6)*	4^+	1394.07(6)*	6.8(4)	1510.11	4^+
2915.1(2)	2^+	2127.6(2)	6.9(4)	787.45	2^+
2955.8(1)*	$3^{(+)}$ *	1445.7(2)*	3.1(2)	1510.11	4^+
		1523.4(2)*	4.2(2)	1432.28	2^+
2962.53(2)	3^-	399.9(2)*	0.37(2)	2562.52	3^+
		629.4(3)*	0.26(2)	2333.58	4^+
		755.7(2)*	0.42(3)	2206.90	2^+
		944.90(3)	6.8(4)	2017.65	3^-
		1203.96(4)*	4.3(2)	1758.55	2^+
		1452.46(3)	7.5(4)	1510.11	4^+
		2175.04(3)	7.8(5)	787.45	2^+
2976.96(9)	4^+	1466.85(8)	7.5(4)	1510.11	4^+
2979.1(3)*	(4^+)	772.3(5)*	1.9(1)	2206.9	2^+
		1546.7(4)*	1.69(10)	1432.28	2^+
2989.1(2)*		1556.8(2)*	0.62(4)	1432.28	2^+
3020.61(2)	5^-	399.67(4)	0.32(2)	2620.96	5^-
		676.87(4)	0.49(3)	2343.72	6^+
		1002.97(5)	1.63(9)	2017.65	3^-
3021.5(2)	6^+*	1511.4(2)	6.6(6)	1510.11	4^+

TABLE VII. (*Continued.*)

E_i (keV)	I_i^π	E_γ (keV)	I_γ (rel.)	E_f (keV)	I_f^π
3046.24(6)	2^+*	1028.63(6)	1.0(1)	2017.65	3^-
		1287.6(2)	5.8(5)	1758.55	2^+
		2258.6(2)	6.0(6)	787.45	2^+
3051.1(1)	4^+	1541.0(1)	6.9(7)	1510.11	4^+
3067.93(3)	4^-*	446.98(3)	0.6(1)	2620.96	5^-
3104.31(4)*	2^+*	1088(1)*	0.2(1)	2017.65	3^-
		1345.65(8)*	1.4(1)	1758.55	2^+
		2316.95(5)*	4.3(4)	787.45	2^+
		2369.6(2)*	0.3(1)	734.85	0^+
		3104.18(8)	2.2(1)	0.00	0^+
3109.35(3)	3^+*	489.2(1)*	0.5(1)	2619.72	3^+
		602.8(1)*	1.0(1)	2506.85	5^+
		689.4(2)*	0.4(1)	2419.68	4^+
		1004.5(1)*	0.6(1)	2104.89	3^+
		1091.77(4)	7.0(8)	2017.65	3^-
		1599.25(8)	2.3(1)	1510.11	4^+
3122.90(5)*		1690.59(5)*	1.1(1)	1432.28	2^+
3154.95(8)	3^+ *	1050.0(4)	0.4(1)	2104.89	3^+
		1396.4(3)*	1.0(1)	1758.55	2^+
		1644.8(2)*	2.0(1)	1510.11	4^+
		1722.8(3)*	0.5(1)	1432.28	2^+
		2367.5(1)*	3.1(2)	787.45	2^+
3166.09(8)	4^+	746.2(2)	0.6(1)	2419.68	4^+
		1061.3(4)	0.5(1)	2104.89	3^+
		1407.6(2)	1.2(1)	1758.55	2^+
		1656.0(1)	2.9(2)	1510.11	4^+
		2378.7(3)	0.9(1)	787.45	2^+
3196.27(3)	3^- *	1178.60(4)	4.7(3)	2017.65	3^-
		1437.6(2)	1.1(1)	1758.55	2^+
		1686.08(7)	2.4(1)	1510.11	4^+
		2408.95(6)	2.8(2)	787.45	2^+
3207.24(3)*	2^-,3,4, 5^+	411.35(3)*	3.2(2)	2795.9	4^-
		1102.2(1)*	0.6(1)	2104.89	3^+
3211.04(7)	5^- *	1193.40(7)	7.1(4)	2017.65	3^-
3211.58(4)	4^+, 6^+*	878.1(1)	1.4(1)	2333.58	4^+
		1701.48(4)	14.7(9)	1510.11	4^+
3238.1(1)*	2^+ *	1031.4(2)*	0.62(4)	2206.90	2^+
		1220.2(3)*	0.19(1)	2017.65	3^-
		1479.5(1)*	1.3(1)	1758.55	2^+
		2450.7(1)*	2.7(2)	787.45	2^+
		3237.5(4)*	0.63(5)	0.00	0^+
3258.3(2)	(1)	3258.3(2)	0.80(5)	0.00	0^+
3271.86(5)*	4^+ *	476.1(2)*	0.99(6)	2795.9	4^-
		651.1(2)*	0.43(3)	2619.72	3^+
		709.6(1)*	0.59(4)	2562.52	3^+
		765.3(1)*	1.00(6)	2506.85	5^+
		1254.7(1)*	2.2(1)	2017.65	3^-
		1761.2(1)*	3.6(2)	1510.11	4^+
3286.0(1)*	4^+ *	867.7(2)*	2.2(1)	2419.68	4^+
		1268.3(5)*	0.19(1)	2017.65	3^-
		1526.8(2)*	1.07(6)	1758.55	2^+
		1776.1(3)*	0.74(6)	1510.11	4^+
		1853.0(2)*	2.7(2)	1432.28	2^+
3302.7(3)*	(2^+)	2515.2(3)*	0.13(1)	787.45	2^+

also limit multiple solutions obtained from angular correlations, alone.

Spin-parity assignments done in this work mostly agree with the recent compilation [36]. However, there are some differences and additions and we also comment on some particular levels reported in Refs. [36,38,39]:

(1) For the disputed mixing ratio of the 644.85-keV transition, we confirm its large value, reported in Ref. [39], which very well fits the positive-parity solution for the 2^+, 1432.28-keV level, now uniquely determined by our linear polarization.

(2) In the present work we cannot confirm the 1880.86-keV level reported in a previous (n,γ) study with spin $I < 5$ [36]. Because of its low energy such a level would be important for the interpretation of ^{98}Mo. We note that this level was not reported in Refs. [38,39].

(3) Our linear polarization confirms positive parity of the 2104.89-keV level.

(4) Spins and parities of the two close-lying 2333.33-keV, 2^+ and 2333.58-keV, 4^+ levels [36,39] are confirmed with the low value of mixing ratio of the 901.02-keV transition fitting well its linear polarization, which determines the $M1/E2$ character of this transition and positive parity of the 2333.33-keV level. Our mixing ratio for the 823.46-keV decay of the 2333.58-keV level is similar to that reported in Ref. [39]. Linear polarization of all three decays of the 2333.58-keV indicates its 4^+ spin-parity.

(5) Our angular correlation and polarization data for the 909.65-keV transition confirm the 4^+ spin-parity of the 2419.68-keV level. We support the 2^+ spin-parity for the 2418.13-keV level.

(6) The 2562.52-keV level was previously reported with spin-parity (2^-) [36,39]. The present angular correlation and polarization data indicate spin-parity 3^+ for this level. We note that the 2^- assignment would be inconsistent with the 709.6-keV feeding from the 4^+, 3271.86-keV level.

(7) Spin $I = 3$ was reported for the 2572.89-keV level in Ref [39]. The present multipolarity measurement indicate spin-parity 1^- for the 2572.89-keV level.

(8) For the 2812.06-keV level our angular correlation and polarization data indicate spin-parity 2^- instead of values proposed previously [36,39].

(9) There is an inconsistency in the parity assignment to the 2896.89-keV level. On the one hand the polarization suggest negative parity. On the other hand the 792.0-keV decay to the 3^+ level and the large δ values of the 1386.8-keV decay point to positive parity of this level.

(10) For the 3046.24-keV level we propose spin-parity 2^+ instead of 4^+ reported in [36] because the 2258.6-keV decay is of a $\Delta I = 0$ character, as indicated by our angular correlation data. We note that the obtained linear polarization for the 1287.6-keV

TABLE VIII. Angular correlation coefficients for γ-γ cascades in ^{98}Mo from thermal-neutron capture reaction. Symbol D (Q) stands for pure, stretched dipole (quadrupole) transition. New results are indicated with an asterisk.

$E(\gamma_1)$-$E(\gamma_2)$ cascade	A_2/A_0 exp.	A_4/A_0 exp.	Spins in cascade	$\delta_{\rm exp}(\gamma_1)$	χ^2/N
173.3–1546.15	−0.13(3)	0.07(6)	5 → 4 → 2	−0.08(4)	1.44
259.11–1023.73	−0.078(8)	−0.04(2)	3 → 2 → 0	−0.01(1)*	3.54
326.23–1432.33	0.37(3)	−0.18(8)	2 → 2 → 0	−0.17(6)*	5.40
335.23–833.61	0.20(4)	0.1(1)	6 → 6 → 4	D	1.31
350.97–713.86	0.25(2)	−0.08(5)	4 → 4 → 4	−0.07(7)	2.13
399.67–603.5	0.26(4)	−0.01(9)	5 → 5 → 3	−0.3(2)*	0.72
434.29–1546.15	0.16(4)	−0.04(9)	4 → 4 → 2	0.0(1)*	0.93
446.98–603.5	0.17(3)	−0.13(7)	4 → 5 → 3	−4.3(9)*	0.00
530.85–1432.33	0.32(9)	1.3(2)	0 → 2 → 0	Q*	0.60
575.1–1758.7	0.18(4)	−0.07(9)	4 → 2 → 0	Q*	4.79
603.5–1230.16	−0.10(2)	−0.05(5)	5 → 3 → 2	Q*	1.56
644.85–787.45	−0.315(5)	0.19(1)	2 → 2 → 0	1.30(7)	2.65
661.14–1023.73	0.13(5)	−0.2(1)	4 → 2 → 0	Q	2.76
672.58–1432.33	−0.02(1)	−0.08(4)	3 → 2 → 0	4.1(4)*	0.01
676.87–833.61	−0.12(4)	−0.18(8)	5 → 6 → 4	6.9(26)*	0.70
713.86–722.66	−0.063(9)	0.01(2)	4 → 4 → 2	0.75(4)*	5.03
			3 → 4 → 2	−0.09(1)*	0.08
722.66–787.45	0.101(4)	−0.01(1)	4 → 2 → 0	Q*	3.65
791.72–1432.33	0.10(2)	−0.04(4)	4 → 2 → 0	Q	1.19
			3 → 2 → 0	0.24(3)	0.54
791.99–672.58	0.07(4)	−0.1(1)	5 → 3 → 2	Q*	1.35
803.9–1023.73	0.20(6)	−0.1(2)	2 → 2 → 0	0.06(8)*	0.31
814.34–1023.73	−0.05(2)	−0.06(5)	1 → 2 → 0	−0.17(2)*	0.42
823.46–722.66	0.25(1)	−0.01(3)	4 → 4 → 2	−0.55(3)*	0.92
833.61–722.66	0.10(1)	1.07(2)	6 → 4 → 2	Q	0.88
901.02–1432.33	0.28(3)	0.05(8)	2 → 2 → 0	−0.05(5)	0.31
909.65–722.66	0.25(1)	−0.01(3)	4 → 4 → 2	−0.3(1)*	0.58
944.9–1230.16	0.06(3)	−0.02(6)	3 → 3 → 2	0.63(9)*	0.13
971.1–787.45	0.444(8)	0.13(2)	2 → 2 → 0	−1.02(5)*	3.22
975.29–722.66	0.25(2)	−0.08(6)	3 → 4 → 2	−0.55(6)	0.39
985.8–1432.33	0.20(9)	−0.1(1)	2 → 2 → 0	D*	1.38
987.32–1432.33	0.20(9)	−0.1(1)	4 → 2 → 0	Q*	1.38
996.9–722.66	−0.43(2)	−0.07(3)	5 → 4 → 2	−1.4(3)	1.03
				−0.9(1)	2.06
1002.97–1230.16	−0.02(5)	−0.1(1)	5 → 3 → 2	Q	3.45
1053.07–1432.33	−0.59(3)	−0.04(6)	3 → 2 → 0	−1.2(2)	3.96
1091.77–1230.16	0.14(3)	−0.02(6)	2 → 3 → 2	D*	0.12
			3 → 3 → 2	7(3)*	0.11
				1.0(2)*	0.11
			4 → 3 → 2	−0.14(5)*	0.11
1093.46–1432.33	0.19(3)	0.01(7)	2 → 2 → 0	0.08(4)	0.03
1110.85–722.66	−0.06(1)	−0.01(3)	5 → 4 → 2	D*	0.44
1140.56–1432.33	−0.06(4)	0.0(1)	1 → 2 → 0	−0.16(4)*	0.28
1168.52–722.66	0.07(3)	−0.02(8)	6 → 4 → 2	Q	0.87
1178.6–1230.16	−0.10(3)	−0.03(7)	3 → 3 → 2	−2.1(4)*	0.12
				0.2(8)*	0.12
1187.46–1432.33	0.17(4)	−0.11(9)	3 → 2 → 0	1.7(3)	0.23
				0.39(9)	1.02
1193.4–1230.16	−0.12(3)	−0.02(6)	5 → 3 → 2	Q*	1.73
1230.16–787.45	−0.098(5)	−0.02(1)	3 → 2 → 0	−0.04(1)*	3.71
1250.03–787.45	0.35(3)	1.03(8)	0 → 2 → 0	Q*	2.11
1257.73–722.66	0.17(3)	0.04(8)	4 → 4 → 2	D*	0.74
1285.8–722.66	0.19(1)	−0.01(3)	4 → 4 → 2	0.01(4)	0.14
1287.6–1023.73	0.14(3)	−0.01(8)	2 → 2 → 0	0.14(4)*	0.06
1317.44–787.45	0.12(1)	−0.09(2)	3 → 2 → 0	2.14(9)*	1.15

TABLE VIII. (*Continued*.)

$E(\gamma_1)$-$E(\gamma_2)$ cascade	A_2/A_0 exp.	A_4/A_0 exp.	Spins in cascade	$\delta_{\exp}(\gamma_1)$	χ^2/N
1335.49–1432.33	0.08(5)	0.0(1)	$4 \to 2 \to 0$	Q*	0.22
1345.65–1023.73	0.16(6)	0.1(2)	$2 \to 2 \to 0$	0.12(8)*	0.46
				−3.1(9)*	1.46
1386.8–722.66	0.14(3)	−0.10(7)	$5 \to 4 \to 2$	2.2(4)	0.49
				0.36(7)*	1.64
1394.07–722.66	0.23(2)	0.02(6)	$4 \to 4 \to 2$	−0.1(1)*	0.08
1419.45–787.45	0.38(1)	0.01(3)	$2 \to 2 \to 0$	−0.20(2)	0.03
1436.55–787.45	0.07(2)	−0.06(5)	$4 \to 2 \to 0$	Q	5.83
			$3 \to 2 \to 0$	2.7(2)*	0.09
1445.7–722.66	0.12(3)	−0.07(7)	$3 \to 4 \to 2$	−0.32(4)*	0.59
1452.46–722.66	−0.17(2)	−0.04(4)	$3 \to 4 \to 2$	0.03(2)*	1.03
1466.85–722.66	0.14(2)	0.02(5)	$4 \to 4 \to 2$	0.17(6)*	0.04
				−1.3(2)*	2.55
1479.5–1023.73	0.21(7)	0.0(2)	$2 \to 2 \to 0$	0.06(9)*	0.02
1511.4–722.66	0.10(2)	0.01(6)	$6 \to 4 \to 2$	Q	0.02
1523.4–1432.33	−0.15(4)	−0.04(9)	$3 \to 2 \to 0$	−0.10(6)*	0.18
1541.0–722.66	0.17(2)	−0.05(6)	$4 \to 4 \to 2$	0.08(7)*	0.88
1546.15–787.45	0.093(9)	−0.01(2)	$4 \to 2 \to 0$	Q	1.74
1546.7–1432.33	0.14(8)	0.1(2)	$4 \to 2 \to 0$	Q*	0.37
1599.25–722.66	0.22(4)	0.0(1)	$2 \to 4 \to 2$	Q*	2.20
			$3 \to 4 \to 0$	−0.48(8)*	0.02
			$4 \to 4 \to 0$	−0.07(2)*	0.25
				−0.8(3)*	1.15
1630.7–787.45	0.18(8)	0.0(2)	$2 \to 2 \to 0$	0.09(10)*	1.06
1632.15–787.45	0.10(7)	−0.1(2)	$4 \to 2 \to 0$	Q*	0.34
1644.8–722.66	−0.17(4)	−0.02(9)	$3 \to 4 \to 2$	D*	0.83
1656.0–722.66	0.12(2)	0.01(5)	$4 \to 4 \to 2$	0.23(5)*	0.00
1686.08–722.66	0.08(4)	−0.07(9)	$3 \to 4 \to 2$	−0.07(5)*	0.52
1697.9–787.45	−0.35(3)	−0.04(7)	$3 \to 2 \to 0$	−0.38(5)	0.15
1701.48–722.66	0.12(2)	0.00(5)	$6 \to 4 \to 2$	Q*	1.73
			$4 \to 4 \to 2$	0.22(5)*	0.06
1761.2–722.66	0.17(3)	0.02(8)	$4 \to 4 \to 2$	D*	0.87
1740.55–787.45	0.34(4)	0.0(1)	$2 \to 2 \to 0$	−0.13(7)*	0.25
1775.08–787.45	0.19(1)	−0.01(3)	$2 \to 2 \to 0$	0.08(2)	0.12
			$3 \to 2 \to 0$	0.43(4)*	0.01
1785.39–787.45	−0.11(2)	−0.01(4)	$1 \to 2 \to 0$	−0.12(9)	0.04
		Ref. [39]:	$3 \to 2 \to 0$	0.01(6)	
1832.26–787.45	−0.28(2)	−0.06(4)	$3 \to 2 \to 0$	−9.7(23)*	0.48
1853.0–1432.28	0.15(6)	0.0(2)	$4 \to 2 \to 0$	Q*	0.55
1913.38–787.45	0.23(2)	0.0(5)	$2 \to 2 \to 0$	0.02(3)	0.00
1945.1–787.45	0.16(2)	−0.06(5)	$2 \to 2 \to 0$	0.12(3)*	1.89
1980.4–787.45	0.09(2)	−0.01(5)	$4 \to 2 \to 0$	Q	0.31
2024.61–787.45	0.12(2)	−0.04(6)	$4 \to 2 \to 0$	Q*	1.12
			$2 \to 2 \to 0$	0.17(3)*	0.60
2082.58–787.45	−0.01(2)	−0.01(5)	$3 \to 2 \to 0$	0.08(3)*	0.04
2127.6–787.45	0.24(3)	−0.02(6)	$2 \to 2 \to 0$	0.01(4)*	0.08
2175.04–787.45	0.24(3)	0.00(7)	$3 \to 2 \to 0$	0.6(4)*	0.08
				1.1(2)*	0.44
2258.6–787.45	0.27(3)	−0.03(7)	$2 \to 2 \to 0$	−0.02(4)*	0.64
2316.95–787.45	0.22(3)	0.01(8)	$2 \to 2 \to 0$	D*	0.98
2367.5–787.45	−0.33(4)	−0.05(8)	$3 \to 2 \to 0$	−6.0(22)*	0.17
				−0.35(6)*	0.21
2408.95–787.45	−0.07(4)	−0.07(9)	$3 \to 2 \to 0$	D*	0.73
2450.7–787.45	0.26(4)	−0.1(1)	$2 \to 2 \to 0$	D*	1.47
2515.2–787.45	0.21(4)	−0.05(9)	$2 \to 2 \to 0$	0.05(5)*	1.46

TABLE IX. Experimental $P_{\rm exp}(\gamma_1)$ and theoretical $P_{\rm th}(\gamma_1)$ values of linear polarization for the γ_1 (upper) transition in γ_1-γ_2 cascades of ^{98}Mo, obtained in this work.

$E(\gamma_1)$-$E(\gamma_2)$	$P_{\rm exp}(\gamma_1)$	Spin-parity	$\delta_{\rm exp}(\gamma_1)$	$P_{\rm th}(\gamma_1)$
259.11–1023.73	0.16(3)	$3^- \to 2^+ \to 0^+$	−0.01(1)	0.099(4)
326.23–1432.28	0.5(1)	$2^+ \to 2^+ \to 0^+$	−0.17(6)	0.37(3)
434.29–1546.15	0.34(9)	$4^+ \to 4^+ \to 2^+$	0.0	0.327
575.1–1758.7	0.1(1)	$4^+ \to 2^+ \to 0^+$		0.167
644.85–787.45	0.34(2)	$2^+ \to 2^+ \to 0^+$	1.30(7)	0.30(5)
661.14–1023.73	0.4(1)	$4^+ \to 2^+ \to 0^+$		0.167
672.58–1432.28	−0.52(8)	$3^+ \to 2^+ \to 0^+$	4.1(4)	−0.44(1)
713.86–722.66	0.27(3)	$4^+ \to 4^+ \to 2^+$	0.75(4)	0.22(6)
		$3^- \to 4^+ \to 2^+$	−0.09(1)	0.24(1)
722.66–787.45	0.26(1)	$4^+ \to 2^+ \to 0^+$		0.167
791.72–1432.28	0.17(7)	$4^+ \to 2^+ \to 0^+$		0.167
		$3^- \to 2^+ \to 0^+$	0.24(3)	0.22(2)
803.9–1023.73	0.5(2)	$2^+ \to 2^+ \to 0^+$	0.06(8)	0.44(2)
814.34–1023.73	0.35(9)	$1^- \to 2^+ \to 0^+$	−0.17(2)	0.45(2)
823.46–722.66	0.40(5)	$4^+ \to 4^+ \to 2^+$	−0.55(3)	0.16(2)
833.61–722.66	0.24(5)	$6^+ \to 4^+ \to 2^+$		0.167
901.02–1432.28	0.3(1)	$2^+ \to 2^+ \to 0^+$	−0.05(5)	0.42(3)
909.65–722.66	0.15(5)	$4^+ \to 4^+ \to 2^+$	−0.3(1)	0.25(4)
944.9–1230.16	−0.6(2)	$3^- \to 3^- \to 2^+$	0.63(9)	−0.20(1)
971.1–787.45	0.07(3)	$2^+ \to 2^+ \to 0^+$	−1.02(5)	0.06(1)
975.29–722.66	−0.8(1)	$3^+ \to 4^+ \to 2^+$	−0.55(6)	−0.42(2)
996.9–722.66	−0.08(7)	$5^+ \to 4^+ \to 2^+$	−1.4(3)	−0.02(2)
		$5^+ \to 4^+ \to 2^+$	−0.9(1)	0.01(1)
1053.07–1432.28	−0.2(1)	$3^+ \to 2^+ \to 0^+$	−1.2(2)	−0.05(2)
1091.77–1230.15	0.33(12)	$2^+ \to 3^- \to 2^+$	D*	0.23(2)
		$3^+ \to 3^- \to 2^+$	7(3)	0.11(2)
			1.0(2)	−0.16(2)
		$4^+ \to 3^- \to 2^+$	−0.14(5)	0.05(1)
1093.46–1432.28	0.5(1)	$2^+ \to 2^+ \to 0^+$	0.08(4)	0.44(1)
1110.85–722.66	0.4(1)	$5^- \to 4^+ \to 2^+$	0.0	0.103
1140.56–1432.28	0.6(2)	$1^- \to 2^+ \to 0^+$	−0.16(4)	0.45(3)
1230.16–787.45	0.17(2)	$3^- \to 2^+ \to 0^+$	−0.04(1)	0.090(3)
1285.8–722.66	−0.27(5)	$4^- \to 4^+ \to 2^+$	0.01(4)	−0.33(1)
1287.6–1023.73	−0.2(2)	$2^+ \to 2^+ \to 0^+$	0.14(4)	0.45(3)
1317.44–787.45	−0.37(4)	$3^+ \to 2^+ \to 0^+$	2.14(9)	−0.51(1)
1386.8–722.66	0.4(1)	$5^- \to 4^+ \to 2^+$	2.2(4)	0.37(2)
		$5^- \to 4^+ \to 2^+$	0.36(7)	0.25(3)
1394.07–722.66	0.5(1)	$4^+ \to 4^+ \to 2^+$	−0.1(1)	0.31(3)
1419.45–787.45	0.53(6)	$2^+ \to 2^+ \to 0^+$	−0.20(2)	0.36(1)
1436.55–787.45	0.05(11)	$4^+ \to 2^+ \to 0^+$		0.167
		$3^+ \to 2^+ \to 0^+$	2.7(2)	−0.48(1)
1445.7–722.66	0.0(1)	$3^+ \to 4^+ \to 2^+$	−0.32(4)	−0.34(3)
1452.46–722.66	0.33(9)	$3^- \to 4^+ \to 2^+$	0.03(2)	0.2(2)
1466.85–722.66	0.7(1)	$4^+ \to 4^+ \to 2^+$	0.17(6)	0.33(1)
		$4^+ \to 4^+ \to 2^+$	−1.3(2)	−0.02(1)
1511.4–722.66	0.1(1)	$6^+ \to 4^+ \to 2^+$		0.167
1523.4–1432.28	0.2(2)	$3^+ \to 2^+ \to 0^+$	−0.10(6)	−0.07(3)
1541.0–722.66	0.3(1)	$4^+ \to 4^+ \to 2^+$	0.08(7)	0.33(1)
1546.15–787.45	0.34(4)	$4^+ \to 2^+ \to 0^+$		0.167
1599.25–722.66	−0.6(2)	$2^+ \to 4^+ \to 2^+$	0.0	0.384
		$3^+ \to 4^+ \to 0^+$	−0.48(8)	−0.40(2)
		$4^- \to 4^+ \to 0^+$	−0.07(2)	−0.32(3)
			−0.8(3)	−0.10(1)
1701.48–722.66	0.4(1)	$6^+ \to 4^+ \to 2^+$	0.0	0.167
		$4^+ \to 4^+ \to 2^+$	0.22(5)	0.33(3)
1740.55–787.45	0.1(2)	$2^+ \to 2^+ \to 0^+$	−0.13(7)	0.39(3)

TABLE IX. (*Continued.*)

$E(\gamma_1)$-$E(\gamma_2)$	$P_{\rm exp}(\gamma_1)$	Spin-parity	$\delta_{\rm exp}(\gamma_1)$	$P_{\rm th}(\gamma_1)$
1775.08–787.45	−0.12(6)	$2^+ \to 2^+ \to 0^+$	0.08(2)	0.44(1)
		$3^+ \to 2^+ \to 0^+$	0.43(4)	−0.32(2)
1785.39–787.45	0.45(8)	$1^- \to 2^+ \to 0^+$	−0.12(9)	0.42(7)
1832.26–787.45	−0.01(9)	$3^+ \to 2^+ \to 0^+$	−9.7(23)	−0.28(2)
1913.38–787.45	0.45(9)	$2^+ \to 2^+ \to 0^+$	0.02(3)	0.43(6)
1945.1–787.45	0.5(1)	$2^+ \to 2^+ \to 0^+$	0.12(3)	0.45(1)
1980.4–787.45	0.3(1)	$4^+ \to 2^+ \to 0^+$		0.167
2024.61–787.45	−0.5(1)	$4^+ \to 2^+ \to 0^+$		0.167
		$2^- \to 2^+ \to 0^+$	0.17(3)	−0.45(1)
2082.58–787.45	−0.2(1)	$3^+ \to 2^+ \to 0^+$	0.08(3)	−0.14(2)
2127.6–787.45	0.2(1)	$2^+ \to 2^+ \to 0^+$	0.01(4)	0.43(1)
2175.04–787.45	0.9(2)	$3^- \to 2^+ \to 0^+$	0.6(4)	0.4(2)
		$3^- \to 2^+ \to 0^+$	1.1(2)	−0.5(1)
2258.6–787.45	0.59(16)	$2^+ \to 2^+ \to 0^+$	−0.02(4)	0.42(1)

decay of this level is not consistent with the 2^+ and 4^+ solutions.

(11) For the 3067.93-keV level we propose spin-parity 4^-, indicated by angular correlations. This replaces the (3^-) assignment reported in [36] and is consistent in with 4^-,5 solutions proposed in [39].

(12) A new $3^{(+)}$ level is proposed at 2955.76 keV and new 2^+ level is proposed at 3104.31 keV.

(13) Our multipolarity data for the 1091.77- and 1599.25-keV decays of the 3109.35-keV level indicate spin-parity 3^+ for this level.

(14) The 6^+ spin-parity is preferred for the 3211.58-keV level as it does not decay to any 2^+ level.

(15) In Refs. [36,47] a 3257.86-keV level with spin $I = 1$ was reported. Such a level should be populated in the ^{97}Mo$(n_{\rm th}, \gamma)^{98}$Mo reaction. In our data there is a 3258.3-keV line and we introduce tentatively a level at 3258.3 keV. However, our data suggest that the 3257.3-keV line may correspond to a primary transition feeding the 5384.4-keV level [23].

(16) Low-spin levels at 2856.2(2), 3010.92, 3095.80, 3229.17, 3241.2, and 3264.9 keV, reported in Ref. [36], are not seen in the present work.

(17) Of other levels discussed in Ref. [39] our angular correlation and polarization data uniquely confirm spin-parity 3^+ of the 2485.43-keV level, spin-parity 5^+ of the 2506.85-keV level, spin-parity 2^+ of the 2700.82-keV level with $\delta = 0.02(3)$ for the 1913.38-keV transition, spin-parity 2^+ of the 2732.55-keV level with $\delta = 0.12(3)$ of the 1945.1-keV transition, and spin-parity 3^+ of the 2870.02-keV level with $\delta = 0.08(3)$ of the 2082.58-keV transition.

III. DISCUSSION

It was proposed in Ref. [10] that the onset of deformation in mass $A \approx 100$ nuclei around neutron number $N = 59$, observed as a function of increasing neutron number i,s helped by the $9/2^+[404]$ neutron extruder [6,7]. As discussed further in Ref. [12], this effect is superimposed on a more gradual process due to the SOP mechanism [14,15]. Such a scenario is supported by analogous observations in mass $A \approx 150$ nuclei, where sudden onset of deformation is helped by the $11/2^-[505]$ neutron extruder [48,49]. It was further proposed that in addition to the $11/2^-[505]$ neutron extruder the $9/2^+[404]$ *proton* extruder acts analogously along isotonic lines in the mass $A \approx 150$ region (see Fig. 7 in Ref. [11]).

The increase of the level density above $Z = 40$ shown in Fig. 1 suggests that also in the mass $A \approx 100$ region one may observe an "extruder-type" action along isotonic lines. The $7/2^-[303]$ proton extruder, originating from the $f_{7/2}$ shell below $Z = 28$ is too low on the single-particle (s.-p.) energy scale to be involved. However, one sees in Fig. 8(a) the $3/2^-[301]$, $5/2^-[303]$, and $1/2^-[301]$ upsloping proton orbitals crossing three downsloping orbitals of $\pi g_{9/2}$ origin, which can act similarly to an extruder orbital. We note that, due to a large number of crossing levels, the "extruder-type" action along Z is spread over a wider range of protons, compared to the "sudden" action of a single $\nu 9/2^+[404]$ extruder along N. This is supported by Fig. 6 of Ref. [10], showing

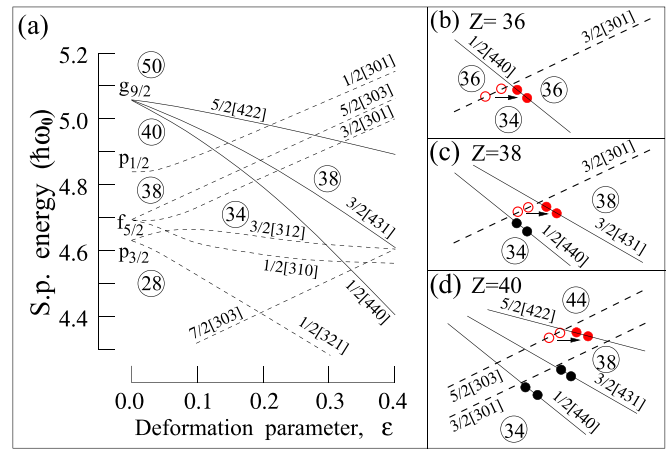

FIG. 8. The Nilsson diagram for protons drawn after Fig. 9 of Ref. [50].

wide minima in the excitation energy of 0^+ levels, produced by shifting proton pairs between crossing levels, as sketched in Figs. 8(b)–8(d). One sees that with the increasing Fermi level more active proton configurations appear. Because of their similar structure, they can mix, further increasing the number of possible low-energy excitations, which is reflected in the growing level density, from the rather "simple" ^{92}Kr to the more collective ^{98}Mo and ^{100}Ru, as shown in Fig. 1.

In the following we will discuss in more detail the information on the $N = 56$ isotones, including our results. Special attention will be paid to the effect of possible phase transitions and shape coexistence phenomena in the region [51,52]. To learn more about the microscopic structure of the $N = 56$ isotones the experimental data will be compared against large-scale shell-model (LSSM) calculations, analogous to those performed in Refs. [12,53,54] for strontium and zirconium isotopes.

A. ^{92}Kr

The ^{92}Kr nucleus displays features characteristic of a soft vibrator with the $R_{42} = E_{\rm exc}(4_1^+)/E_{\rm exc}(2_1^+)$ ratio of 2.34. Except for a short ground-state cascade, no other structures are evident below 7 MeV of excitation. An indication of an emerging γ-type collectivity is the 3^+, 2066.3-keV and 5^+, 2492.0-keV levels. No negative-parity excitations were identified in this nucleus.

Figure 9 compares experimental excitations with the present LSSM calculations. The parentheses indicate a tentative assignment and the horizontal bars indicate unknown spin with value within the range of the bar. We note that the LSSM calculations do not predict any spin $I = 1$ level below 5 MeV of excitation.

The vibrational nature of ^{92}Kr is supported by the linear increase of excitation energies as a function of spin for the near-yrast levels, which follow the dashed line. Generally, all experimental levels have their counterparts calculated nearby. It is of interest to verify possible 0^+ excited levels predicted by the LSSM but not observed experimentally to date.

To learn more about ^{92}Kr we inspected LSSM wave functions. Table X shows occupations of neutron and proton orbitals in ^{92}Kr obtained in the calculation. Of the six valence neutrons approximately four occupy the $d_{5/2}$ shell and one occupies the $s_{1/2}$ shell, while the remaining neutron is distributed among the $g_{7/2}$, $d_{3/2}$, and $h_{11/2}$ shells, the latter containing no more than 0.2 neutron particles, on average. On the proton side, out of the eight valence particles, on average three are in the $p_{3/2}$ shell, four in the $f_{5/2}$ shell, one in the $p_{1/2}$ shell, and a small fraction in the $g_{9/2}$ shell. Some notable deviations from these average numbers are indicated in bold.

In the last column of Table X we show the fraction of the wave function corresponding to summed contributions of main s.-p. configurations, contributing at least 5%, each. For example, the wave function of the 0_1^+ ground state contains three such configurations, $[\nu d_{5/2}^6 \otimes \pi(p_{3/2}^4 + f_{5/2}^4)]$, $[\nu d_{5/2}^6 \otimes \pi(p_{3/2}^2 + f_{5/2}^4 + p_{1/2}^2)]$, and $[\nu(d_{5/2}^4 + s_{1/2}^2) \otimes \pi(p_{3/2}^4 + f_{5/2}^4)]$, contributing 9%, 8%, and 7%, respectively, which sums to 24% shown in the last column. The remaining 76% of the wave function is composed of many other configurations with small contributions. In this context, the 0_2^+ and 0_3^+ levels (not yet known experimentally) are of more s.-p. nature than the 0_1^+ ground state.

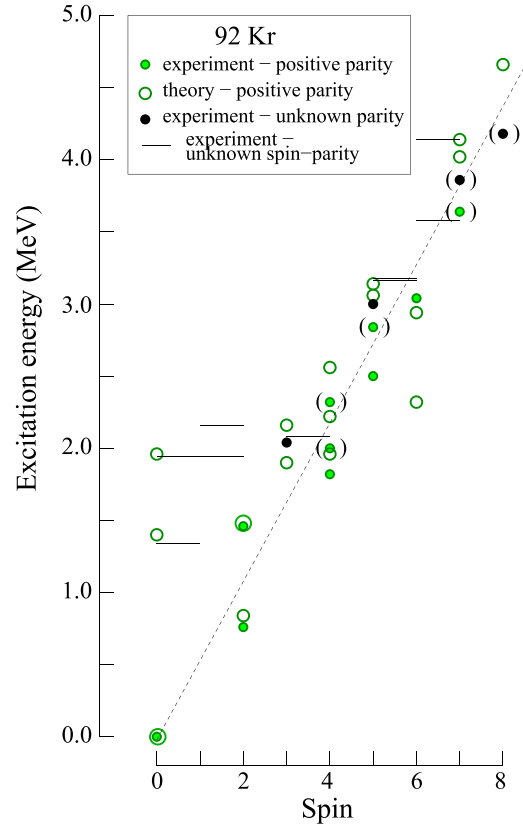

FIG. 9. Experimental excited levels in ^{92}Kr, as shown in Fig. 4 compared to the LSSM calculations. See text for more comments.

We note that, generally, wave functions of levels in ^{92}Kr shown in Table X are composed of many configurations with small contributions. This "collectivity" is higher here than in the ^{94}Sr isotone. For example, in the 2^+ levels the total of main s.-p. contributions in ^{92}Kr is three times lower than in ^{94}Sr (see Table XVI in Ref. [12]), suggesting that ^{92}Kr is more collective than ^{94}Sr. This may be due to the $Z = 40$ subshell closure, which influences ^{94}Sr more than ^{92}Kr. On the other hand this higher "collectivity" of ^{92}Kr does not help the formation of band structures, which seem better developed in ^{94}Sr [12]. One notes that in ^{94}Sr the calculated population of the $g_{9/2}$ proton shell is, on average, higher [12] than in ^{92}Kr, which helps the formation in ^{94}Sr of near-yrast medium-spin band members and deformed intruder configurations. In contrast, levels in ^{92}Kr, dominated by excitations within the f-p shells, are more of a vibrational nature and, as reported before [18,55], the deformation onset is slower in Kr isotopes as compared to Sr isotopes.

B. ^{94}Sr

In the ^{94}Sr nucleus, which was discussed in detail in recent works [12,53], the $R_{42} = 2.56$ value is higher, suggesting its transitional character. One observes here a positive-parity cascade, which is probably due to a developing γ collectivity.

TABLE X. Occupation of neutron and proton orbitals in selected levels of ^{92}Kr. Notable deviations from average occupation are indicated in bold. See text for more comments.

	E_{exc}	Neutrons					Protons				Main	Total main
I^π	(keV)	$d_{5/2}$	$s_{1/2}$	$g_{7/2}$	$d_{3/2}$	$h_{11/2}$	$p_{3/2}$	$f_{5/2}$	$p_{1/2}$	$g_{9/2}$	s.-p.	s.-p.
0_1^+	0	4.42	0.74	0.24	0.36	0.24	2.88	3.85	0.89	0.39		0.24
		6	0	0	0	0	4	4	0	0	0.09	
		6	0	0	0	0	2	4	2	0	0.08	
		4	2	0	0	0	4	4	0	0	0.07	
0_2^+	1309	4.25	1.16	0.18	0.26	0.16	2.97	3.83	0.85	0.35		**0.39**
0_3^+	1951	4.24	1.01	0.23	0.30	0.21	3.49	2.81	1.47	0.23		**0.42**
2_1^+	854	4.16	1.04	0.21	0.40	0.19	3.01	3.68	0.97	0.34		0.13
2_2^+	1461	4.24	0.95	0.21	0.38	0.21	3.12	3.76	0.85	0.27		**0.06**
3_1^+	1896	4.30	1.01	0.17	0.37	0.15	3.09	3.71	0.90	0.30		0.14
3_2^+	2156	4.28	0.98	0.18	0.39	0.16	3.11	3.64	0.96	0.29		0.24
4_1^+	1986	4.02	1.26	0.18	0.39	0.15	3.10	3.56	1.04	0.30		0.19
4_2^+	2244	4.38	0.74	0.23	0.43	0.23	2.94	4.05	0.70	0.31		0.09
5_1^+	3047	3.87	0.67	**0.99**	0.31	0.15	2.89	3.83	0.85	0.43		0.16
5_2^+	3122	4.23	1.04	0.19	0.37	0.16	3.01	3.74	1.00	0.25		**0.07**
6_1^+	2328	4.01	0.98	0.24	**0.60**	0.16	3.00	3.75	0.92	0.33		**0.05**
6_2^+	2934	3.97	0.82	0.39	**0.63**	0.19	2.94	3.95	0.76	0.34		**0.00**
7_1^+	4024	4.58	0.86	**1.06**	0.36	0.09	2.86	4.48	0.47	0.19		**0.44**
7_2^+	4139	4.15	0.64	0.88	0.24	0.09	3.08	3.81	0.93	0.17		0.20
8_1^+	4654	3.57	0.94	**1.05**	0.28	0.16	3.09	3.66	0.94	0.31		0.13

A strongly populated cascade of negative parity states, which dominates the yrast excitation scheme, is most likely due to octupole collectivity building up thanks to the $\pi g_{9/2}$–$\pi p_{3/2}$ proximity.

C. ^{96}Zr

The double closure of the $\nu d_{5/2}$ and $\pi g_{9/2}$ subshells, on one hand, and the emerging collectivity due to an increasing number of valence nucleons, on the other hand, make the $^{96}_{40}Zr_{56}$ nucleus a very special case with a possible triple-shape coexistence, as suggested by model calculations [56].

The ground-state cascade in ^{96}Zr, characteristic of a spherical nucleus, is most likely dominated by the $(\pi g_{9/2})^2 \otimes (\nu d_{5/2})^2$ and $(\pi g_{9/2})^2 \otimes (\nu g_{7/2})^2$ s.-p configurations, extending up to spin 14^+. On the other hand, one observes in ^{96}Zr a non-yrast, positive-parity cascade, which suggests an emerging collectivity. With new decays found in the present work, this cascade is even more developed than the analogous cascade in ^{94}Sr.

One notes that the negative-parity cascade in ^{96}Zr is less pronounced than in ^{94}Sr [12]. This may be due to a decreasing contribution from the $\pi g_{9/2}$–$\pi p_{3/2}$, $\Delta j = 3$ pair, as the $\pi p_{3/2}$ orbital is "buried" deeper in the core when the proton number grows. This seems to contradict the results of an extensive analysis of octupole strength in Ref. [57]. However, the very high $E3$ strength reported in the past in ^{96}Zr [57,58] was shown recently to be significantly lower [59].

It was proposed that the 0_2^+ level, the first excited state in ^{96}Zr, is a four-particle, four-hole "intruder" configuration [60,61], resulting from the excitation of a pair of protons across the $Z = 40$ subshell and a pair of neutrons across the $N = 56$ subshell closures [62]. A small deformation, $\beta_2 = 0.2$, was deduced for this configuration [63]. The value $B(E2; 2_2^+ \rightarrow 0_2^+) = 36(11)$ W.u. measured in Ref. [64] was the base for further, moderately successful model descriptions of this structure [65,66], but problems with proper description of the positive-parity cascade remain [67].

The 3^+ level at 2438.8 keV was considered a sign of a nonaxial collectivity in ^{96}Zr, though it could not be well reproduced in the calculations [67]. In the present work we see a link between 3^+ and 5^+ levels, which supports γ collectivity. However, in nuclei from this region one also observes the so-called mixed-symmetry excitations, which produce multiplets including a 3^+ excitation.

The present data seen in Fig. 6 do not show any rotationlike structures on top of any of the excited 0^+ levels in ^{96}Zr. The cascade on top of the 0_2^+ level is just a hint of a band, but its shape does not indicate even a weak deformation. We also could not find any band on top of the 2^+ level at 2668 keV, claimed to be a bandhead in Ref. [65]. In the high-spin study of ^{96}Zr [34] no such structures were seen, either.

The multiple, close lying 4^+, 6^+, and 8^+ levels suggest three "proto" bands in ^{96}Zr: the cascade on top of the ground state, proposed to be due to the $(\pi g_{9/2}^2)_j$ coupling [68], the cascade on top of the 1581.65-keV, 0_2^+ level, and the third cascade starting from the 2438.8-keV, 3^+ level, a possible γ band, with the 2^+ γ bandhead still not known. These three cascades, evidently mixed [57], suggest an emerging collectivity in ^{96}Zr, but as pointed in Ref. [57] their interpretation in terms of bands is not obvious, even with the 6_1^+, 3483.55-keV level being even considered to be a two-octupole phonon excitation [57]. Thus, the scenario of the deformation and the shape coexistence in ^{96}Zr drawn in Ref. [64] may be premature. As stated later in Ref. [65] "the available data do not allow for a unique assignment of the intriguing structure of ^{96}Zr."

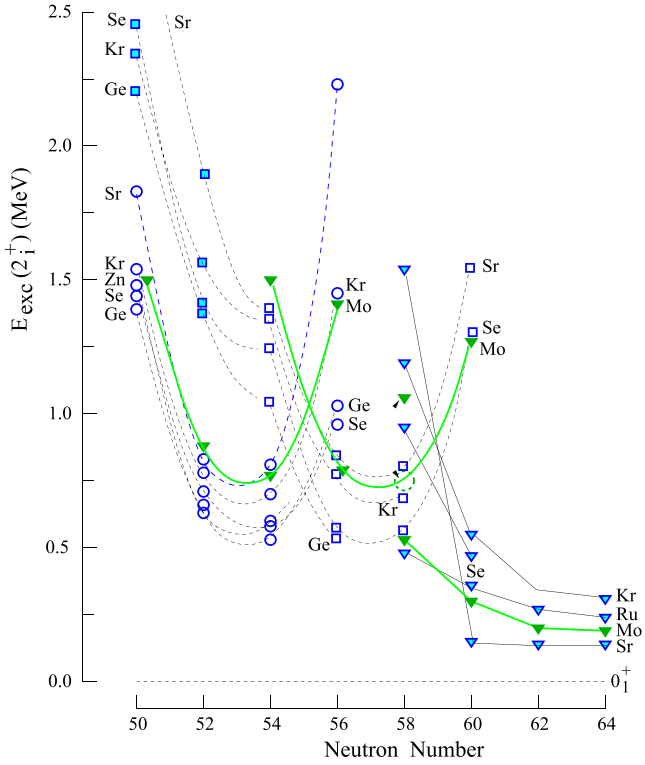

FIG. 10. Excitation energies of 2^+ levels in the $A \approx 100$ region. The data are from the present work and from the ENSDF database [13]. See text and Ref. [12] for more comments.

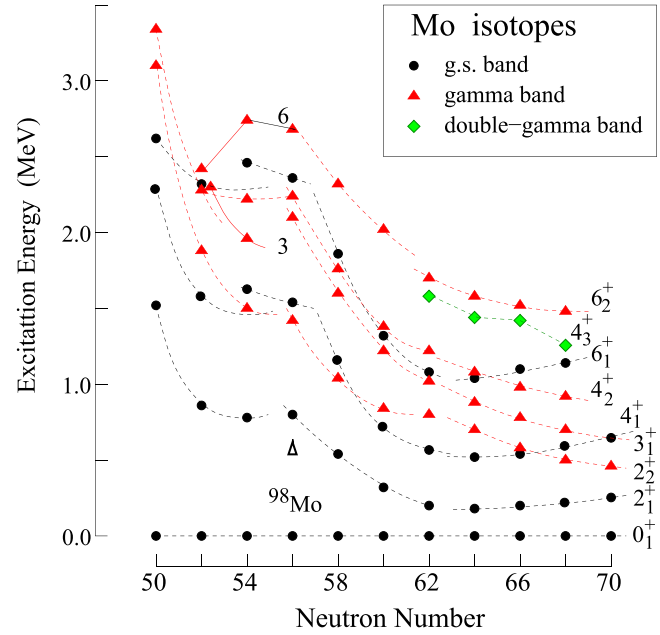

FIG. 11. Excitation energies of selected, low-spin levels in Mo isotopes. The data are from the present work and from the ENSDF database [13]. See text for more comments.

One more comment on ^{96}Zr is that according to Fig. 8 there should be more various excitations in ^{96}Zr than in ^{94}Sr and, accordingly, higher density of low-energy levels. This is not evident in Fig. 1. A possible reason is the strong binding of the ground state in ^{96}Zr, which shifts excited levels up in energy in this nucleus. One notes the rather high number of levels in ^{96}Zr (blue squares) but at higher energy than in ^{98}Mo and ^{100}Ru. With the 2_1^+ excitation energy in ^{96}Zr around 0.7 MeV, as in other isotones, the density distribution in Fig. 1 would look in ^{96}Zr more like in ^{98}Mo and ^{100}Ru, while in ^{94}Sr it is really shifted to higher energy.

D. ^{98}Mo

The excitation scheme of ^{98}Mo shows a much richer set of low-energy excitations as compared to lighter $N = 56$ isotones. The generally lower energies of these excitations also suggest higher collectivity in this nucleus, where previous works discussed a number of various structures. In the following we will review in more detail modes of excitations which may contribute to the development of the collectivity, adding our results. This will be done in a wider context of excitations in $N = 56$ isotones.

1. The ground-state band and 2_1^+ excitations

The $E_{exc}(4_1^+)/E_{exc}(2_1^+)$ ratio in ^{98}Mo of 1.92 suggests a spherical vibrator nature of the ground-state configuration in this nucleus. It is interesting to look at the energies of 2_1^+ levels in Mo isotopes. Figure 10, drawn after Fig. 13 of Ref. [12], now with data for Mo isotopes (green triangles) included, suggests that the nature of 2^+ excitations in Mo is the same as in other isotopic chains of the region (Zr isotopes are not shown).

The shell model analysis presented in Ref. [12] tells that 2^+ excitations in Sr isotopes are predominantly of s.-p. nature and are dominated by the $d_{5/2}$ neutron pair at lower N and by the $g_{7/2}$ neutron pair at higher N. The characteristic U-shape distributions seen in Fig. 10, well reproduced by the shell model, are due to the rising Fermi level (see Fig. 14 and associated comments in Ref. [12]). The energy drop at $N = 60$ is due to lowering of the deformed intruder structure.

The distribution of 2_1^+ and 2_2^+ levels in Mo isotopes is very similar, thus their interpretation is likely the same, with the small difference that the energy drop of deformed structures in Mo happens already at $N = 58$. We note the irregular position of the 2_2^+ level in ^{100}Mo, which may results from the repulsion between the 2_1^+ and 2_2^+ levels. Their displacement suggests a strong interaction of the order of 250 keV (assuming the near degeneracy of the unmixed levels).

The above scenario is supported by the systematic trends shown in Fig. 11. As in Fig. 10 one can distinguish here three regions of the 2_1^+ and the associated 4_1^+ and 6_1^+ excitations in Mo isotopes, the region of s.-p. excitations ($50 \leqslant N \leqslant 54$), the region of the emerging collectivity ($56 \leqslant N \leqslant 62$), and the region of well deformed structures ($N > 62$). The $N = 56$ line is a border line between the first two groups and, as seen in Fig. 11, it is not obvious to which group the $N = 56$ points should be assigned (analogous uncertainty applies to $N = 62$ points). We note that at $N = 64$ (the middle of the 50–82 neutron shell), the 2_1^+ excitation energy reaches a minimum. The slight increase of this energy above $N = 64$ is most likely due to the shape change towards an oblate deformation [69,70].

Finally, we comment on the proton dependence of low-spin excitations in the $N = 56$ isotones, shown in Fig. 12. If not for the deviation at $Z = 40$, due to extraordinary strong binding of the ground state in ^{96}Zr, the dependence of 2^+_1 level on Z would be much weaker and of much different shape than the dependence on N in Figs. 10 and 11.

As concluded in Ref. [16] "there is no comprehensive theoretical explanation for the 2^+ lowest excited state spin and parity dominance in even-even nuclei." The three experimental systematics shown in this section suggest that the 2^+_1 levels in nondeformed nuclei in the region are due to valence neutrons.

2. 0^+ *excitations*

The 0^+ excitations in the region were discussed in our previous paper [10], where the systematics of excitation energies of 0^+ in the $N = 56$ isotones can be seen in Fig. 6. Together with the $N = 58$ chain, these values are the lowest in the region, reaching the minimum at $Z = 42$. The deviation from the regular trend seen in ^{96}Zr may result from an exceptionally low position of the ground state in ^{96}Zr (further studies are needed to explain this effect).

As mentioned above, in addition to the role of the $\nu 9/2^+[404]$ extruder, the shape change in the $A \approx 100$ region is helped by the bunch of $1/2^-[301]$, $3/2^-[303]$, and $5/2^-[303]$ upsloping proton orbitals, which act in the same way as an extruder. These orbitals deliver six extra protons to the Fermi level and pass them to the deformation-driving, downsloping orbitals originating from the $\pi g_{9/2}$ intruder. Consequently, as suggested by Figs. 8(b)–8(d), one expects an increasing number of low-lying 0^+ excitations with the proton number increasing up to $Z = 44$, which is indeed observed in Fig. 12. This mechanism is most effective in ^{98}Mo and ^{100}Ru, which is also reflected in the high density of levels below 4 MeV, seen in the inset of Fig. 1. At higher Z the density of low-energy 0^+ levels may fall. It is of interest to search for further 0^+ levels in ^{102}Pd to verify this suggestion, because Fig. 6 in Ref. [10] hints at another set of 0^+ levels above $Z = 64$, possibly due to hole excitations in the $\pi g_{9/2}$ shell.

The estimated interaction strength between 0^+_1 and 0^+_2 states in ^{98}Mo reported in Ref. [38] is about 380 keV, close to the 326 keV value reported in Ref. [47]. However, Ref. [71] reports a factor of 2 lower mixing potential, stating that "0^+ states are barely mixed" (some problems with the results of Ref. [47] were reported in Ref. [72]).

In Ref. [47] the decay branch of the 3551.2-keV level with spin $I = 1$ and unknown parity (which is not a problem, they said) to 0^+_1 and 0^+_2 states in ^{98}Mo was used to estimate the interaction strength between the two states. In the present work we observe in ^{98}Mo a level at 2508.00 keV with tentative spin $I = (1)$, for which we proposed decays to 0^+_1 and 0^+_2 states. This level is probably the same level as the 2509(2)-keV level with spin-parity $I^\pi = 1^-$, reported in the compilation [36] and could be used to estimate the interaction strength between 0^+_1 and 0^+_2 states.

We applied the schematic analysis proposed in Ref. [47] to the 2508.00-keV level. Using intensities of 1773.0 and 2508.2 keV decays of this level, observed in the present work, we obtained a mixing strength between 0^+_1 and 0^+_2 states in ^{98}Mo of 333 keV, similar to values reported in Refs. [38,47]. (We note that, to make sure we understand the procedure, we have redone the calculation of Ref. [47] using their data. For the decay of the 3290.1-keV level in ^{100}Mo we obtained the same value of 321 keV, but for the decay of the 3551.2-keV level in ^{98}Mo the obtained value of 303 keV, which differs somewhat from the 326-keV strength reported in Ref. [47].)

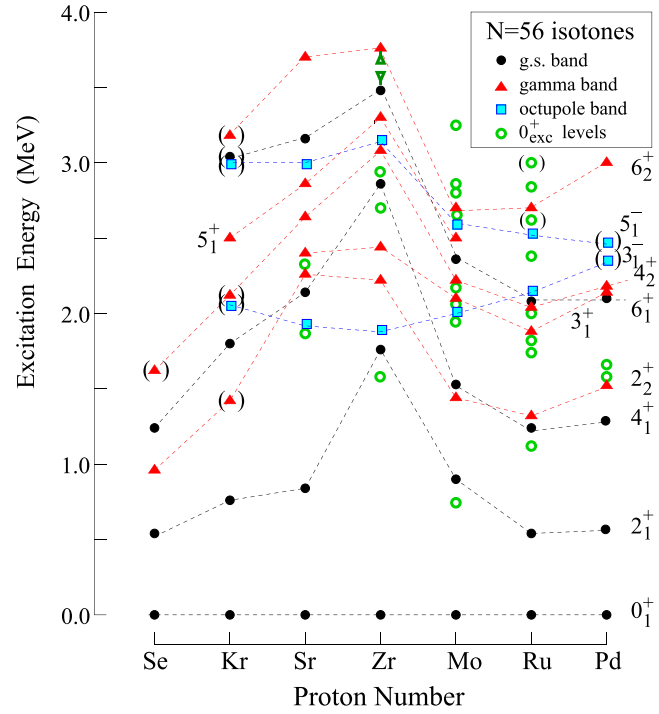

FIG. 12. Excitation energies of selected, low-spin levels in $N = 56$ isotones. The data are from the present work and from the ENSDF database [13]. In the figure the 6^+_1 level is assigned to the ground-state band after Ref. [57]. See text for more comments.

The differences and uncertainties mentioned above stress the need for reliable experimental information about the discussed, low-spin levels in ^{98}Mo. The revised analysis using better data may alter the picture of strong configuration mixing in this nucleus [39,64] and help in understanding the nature of 0^+_2 levels in the region and in ^{98}Mo in particular, where the 0^+_2 energy is exceptionally low. Interestingly, the low mixing between 0^+_1 and 0^+_2 states in ^{98}Mo, reported in Ref. [71], resembles the low mixing between 0^+_1 and 0^+_2 states in ^{98}Sr and ^{100}Zr [10], where it likely results from an admixture of the $\nu 9/2^+[404]$ extruder to these states.

Note the large energy gap between 0^+_2 and 0^+_3 states in ^{98}Mo, which again highlights the extra low excitation energy of the 0^+_2 level in ^{98}Mo, possibly due to the mentioned extruder admixture. Using the present "complete spectroscopy" data we searched for an additional 0^+ level between the two but did not find any.

The 0^+_1 state in ^{98}Mo is proposed to correspond to an intruder (deformed) structure, while the 0^+_2 state should correspond to a spherical configuration [38,39]. Because the 0^+_1 level ^{96}Mo is spherical, this would mean that the swap of the two configurations takes place at much lower N (here $N = 56$)

compared to an analogous change in Sr isotopes observed at $N = 60$ (see Fig. 13 in Ref. [12]). As discussed above, the systematics of Fig. 10 point to such change at $N = 58$ in Mo isotopes, which is consistent with our observations that both 0_1^+ and 0_2^+ states in ^{98}Mo$_{56}$ are rather spherical.

We stress the importance of verifying the shape coexistence details in ^{98}Mo, which will help the understanding of the shape change process in the region. As discussed a long time ago in Ref. [73], this change is either of the first-order ("swap" of the coexisting shapes) or the second-order type (a gradual evolution of the 0_1^+ state, as proposed by Federman and Pittel [14,15]) and the debate is not over.

3. γ collectivity versus mixed-symmetry excitations at $N = 56$

The neutron-rich Mo and Ru isotopes are known to exhibit the highest γ collectivity in the $A \approx 100$ region [74–80], with well developed γ bands and double-γ phonon excitations in ^{104}Mo and higher-Z isotopes, as seen in Fig. 11. The characteristic feature of γ collectivity is 3^+, low-energy excitations. In Fig. 11 they are seen in a wide, $52 \leqslant N \leqslant 70$ range though at significantly varying energies. As in the case of 2_1^+ levels, there are three groups of 3_1^+ levels and the associated levels (the 2_2^+ bandheads and the 4_2^+, 5_1^+, and 6_2^+ members of γ structures): the region of s.-p. excitations at $52 \leqslant N \leqslant 56$, the region of emerging collectivity ($56 \leqslant N \leqslant 62$), and the region of well deformed structures ($N > 62$). Again, the $N = 56$ line marks a border between the first two groups while the $N = 62$ marks a border between the two latter groups.

The well developed γ bands at $N > 62$ decrease in energy, which is consistent with the growing 2_1^+ excitation energy when moving towards an oblate shape. Interestingly, below $N = 64$, the 2_2^+, 3_1^+, 4_2^+, 5_1^+, and 6_2^+ levels, which may be seen as members of developing γ bands, follow closely the systematic trend of levels in ground-state cascades, as seen in both Fig. 11 and Fig. 12. This suggests that these levels, especially at $N < 58$, are predominantly due to excitations of valence neutrons. On the other hand, their collective component develops due to the proton-neutron interaction [2,8] and is helped by the increasing proton number as seen in Fig. 15 of Ref. [12], showing γ bands in Ru isotopes, which at $N < 64$ are developed better than in Mo isotopes.

We note that Refs. [38,39] considered a possible γ softness of the ground state configuration in ^{98}Mo but the 2_2^+, 3_1^+, 4_2^+, and 6_2^+ cascade based on the 1432.28-keV level, which is proposed in the present work as the "proto"-γ band, was not discussed there. Instead, in Ref. [39] possible mixed-symmetry states were proposed. Such structures were reported in ^{94}Mo [81] and in ^{96}Mo [82] with 3_1^+ excitations included. As pointed out in Ref. [39] in ^{98}Mo the situation is not clear in this respect.

In the present work we could determine the positive parity of 2_7^+, 2525.77-keV and 2_9^+, 2700.82-keV levels in ^{98}Mo, which makes the latter level a more reliable candidate for a mixed symmetry state (Q_m) on top of the 0_2^+ configuration. One can also propose candidates for two-phonon, mixed-symmetry states (Q_mQ_s) in ^{98}Mo. The 4^+ level at 2767.68 keV decays to the 2206.90-keV, 2^+ level proposed as the Q_m excitation and is a candidate for the Q_mQ_s state on top of 0_1^+, while the 4^+ level at 2976.96 keV is a candidate for the Q_mQ_s state on top of 0_2^+. We note the proximity of the 3^+ level at 2870.02 keV. One could also consider the 3109.35-keV level as the candidate for the 3^+, Q_mQ_s state on top of 0_2^+. This level decays to the 3^+ level at 2619.72 keV, which might be a candidate for the 3^+, Q_mQ_s state on top of 0_1^+. However, the 3109.35-keV level decays also to the 5^+, 2506.85-keV level, which suggests that the 3109.35-keV level may be rather associated with γ collectivity, which is clearly present in ^{98}Mo because the 3_1^+ level at 2104.89 keV has too low energy to be a Q_mQ_s state. Another problem with mixed symmetry states in ^{98}Mo is the lack of a candidate for the 1^+ member of the Q_mQ_s multiplet, a characteristic, mixed-symmetry excitation, which is not present in γ bands.

We have not discussed the $M1$ strength out of mixed-symmetry states in ^{98}Mo, which should be an important validation factor for these structures. The problem is, that, as pointed out in Ref. [39], this strength could be strongly fragmented, thus not so useful for the validation of mixed-symmetry states. The fragmentation should be due to sizable deformation [39], but as discussed above, the deformation in ^{98}Mo is small. However, as pointed out in Ref. [71], in ^{98}Mo the 2^+ and 4^+ levels exhibit very high interaction and mixing. It could be that the numerous 2^+, 3^+, and 4^+ levels observed in ^{98}Mo and ^{100}Ru above 2 MeV are due to a mechanism yet to be identified, whereas the emergence of γ collectivity at low energies is due to the multilevel mixing of these numerous levels (see, e.g., Sec. 1.5 of Ref. [9]).

4. Negative-parity excitations at $N = 56$

The review [57] reported high octupole collectivity in ^{96}Zr, based on the very large $B(E3)$ of 69(23) W.u. reported in Ref. [58]. Recently, this value with a large uncertainty was corrected to $B(E3) = 42(3)$ W.u. [59], a rate significantly lower though still high. The new value results from the half-life of 67.8 ps measured in Ref. [83], compared to 46(15) ps reported in Ref. [58] (one also notes the half-life of 84(44) ps reported in Ref. [84]). Another input datum is the $E3$ branch of the 3_1^- level in ^{96}Zr, deduced from the intensity ratio of the 1897.30- and 1750.50-keV transitions to be 12.8(3) [59], which is close to the ratio of 12.7(7) used in Ref. [58] and to the present work result of 14.0(5). The present value was obtained by comparing relative γ intensities of 1897.30- and 1750.50-keV transitions, as seen in a γ-ray spectrum doubly gated on the 1222.70- and 363.60-keV lines in a triple-γ histogram.

Strong octupole correlations in ^{96}Zr are due to the proximity of two pairs of $\Delta I = 3$, opposite-parity orbitals, $\nu(d_{5/2}, h_{11/2})$ and $\pi(p_{3/2}, g_{9/2})$, which can be coupled by an octupole operator. The enhanced correlations at $N = 56$, one of the "octupole magic numbers," are supported by calculations [85,86], reporting significant softness against reflection asymmetry at $N = 56$, but not predicting any stable octupole deformation in the region.

It was found in Ref. [59] that the octupole collectivity involves a large number of proton and neutron orbitals. The complex structure of the 3_1^- excitation in ^{96}Zr is supported by the systematic trend of 3_1^- levels in $N = 56$ isotones, shown

in Fig. 12. Unlike the 2_1^+, s.-p. level, the energy of the 3_1^- level does not rise at the $N = 56$ closure of the $\nu d_{5/2}$ shell. The regularity of the trend suggests that the 2045.7- or the 2077.4-keV level in ^{92}Kr may correspond to the 3_1^- excitation (see also comments in the compilation [24]).

In contrast to the 3_1^- levels, the 5_1^- levels show an increase at $N = 56$, which suggests that in ^{96}Zr the 5_1^- excitation may be due to the coupling of 3_1^- and 2_1^+ excitations. The same may apply to lower-Z isotones (the systematics suggests that the 2996.3-keV level in ^{92}Kr corresponds to the 5_1^- excitation). However, it is unlikely to be so in heavier $N = 56$ isotones, especially in ^{102}Pd, where the 5_1^- level is too close in energy to the 3_1^- level to correspond to the $3_1^- \otimes 2_1^+$ coupling.

The numerous 3^- and 5^- levels in ^{98}Mo indicate that, apart from the isoscalar octupole phonon [18], there are other modes of negative-parity excitations at $N = 56$, like the 3^-, isovector excitations [87]. Moreover, s.-p. configurations of negative parity appear at similar energies. For example the $\pi(g_{9/2}, p_{1/2})_{5^-}$ coupling, observed at $N = 50$ in ^{90}Zr and ^{92}Mo may also appear at $N = 56$ as suggested by Fig. 20 of Ref. [12].

With the suggested contribution of the $\nu(d_{5/2}, h_{11/2})$, $\Delta I = 3$ pair to the enhanced octupole collectivity in ^{96}Zr one could expect the presence of the $h_{11/2}$ neutrons among active valence orbitals. However, we could not identify in ^{96}Zr the characteristic, $\nu(g_{7/2}, h_{11/2})_{9^-}$ excitation, which serves as a useful test of the $\nu h_{11/2}$ energy in the region [88]. Such an excitation was observed at 4858.9 keV in ^{94}Sr [88] and at 3524.7 keV in ^{96}Sr [12] and was also proposed at 4197.9 keV in ^{98}Zr [89]. Thus, it could be expected in ^{96}Zr at about 5 MeV. The 4846.2-keV level is a possible candidate, but it may be located at higher energy. As reported in Ref. [90] the $\nu h_{11/2}$ energy shows a significant increase in the ^{97}Zr, odd-N neighbor, compared to lighter Zr isotopes, and the 2264-keV level, reported previously with spin $(11/2^-)$ was proposed to have spin-parity $9/2^+$, instead [91].

IV. SUMMARY AND PERSPECTIVES

In summary, the main goal of the work was the study of the evolution of collectivity with the growing proton number in the region and finding how this is related to the population of the $\pi g_{9/2}$ shell and what is the mechanism of this population. For this reliable spin-parity assignments to known excited levels and the identification of new levels were needed. To obtain such information excited levels in ^{92}Kr, ^{96}Zr, and ^{98}Mo, $N = 56$ isotones were studied in measurements of γ rays following neutron-induced fission of ^{235}U and neutron-capture on a ^{97}Mo target, performed using the EXILL and FIPPS multidetector Ge arrays, respectively.

A total of 16 new levels, 64 new or corrected decays, and 35 new or improved spin-parity assignments were obtained in the three nuclei. Precise angular correlations and linear-polarization correlations measured in this work were used to determine new spin-parity assignments and verify previously published ones. All linear-polarization values are new.

The improved data allowed us to build extensive experimental systematics, which helped us to discuss the evolution of collectivity in the region and in $N = 56$ isotones, in particular. To learn more about the microscopic structure of levels at $N = 56$, large-scale shell-model calculations were also performed and the results compared to experimental data in ^{92}Kr.

It is proposed that the population of the $\pi g_{9/2}$ shell in the $A \approx 100$ region is helped by crossing of the low-Ω p-f upsloping orbitals, which deliver extra protons to the Fermi surface. Pairs of protons from the p-f orbitals, passed to the low-Ω orbitals generate 0^+ excitations, of predominantly 2p-2h, proton structure. This mechanism explains the increasing number of low-energy 0^+ excitations at $N = 56$ when the proton number grows. The 0_1^+ and the 0_2^+ levels, which show some collectivity, may result from the multilevel mixing of the many higher-lying 0^+ excitations. The 0_2^+ level in ^{98}Mo may also contain an admixture of the neutron $9/2^+[404]$ extruder orbital.

The large number of active orbitals at the Fermi level also explains the increased level density in ^{98}Mo and ^{100}Ru. The numerous 2^+ and 4^+ levels seen around 3 MeV of excitation energy are likely due to s.-p. excitations of these orbitals, similar to the predominantly s.-p. nature of 2_1^+ levels in the region. The new effect observed in ^{98}Mo is the cascade on top of the 2_2^+ level at 1432.28 keV, proposed to be a "proto"-γ band. This low-energy structure probably emerges from the multilevel mixing of the 2^+ and 4^+ s.-p. excitations present around 3 MeV. Theoretical verification of this or proposing another mechanism is needed.

The $N = 56$ isotones and the ^{98}Mo nucleus in particular are a convenient place to study the role of s.-p. excitations in the emergence and the evolution of collective effects. It is of high interest to verify the picture proposed in this work, in particular the degree of deformation of 0_1^+ and 0_2^+ states. Further analysis of our ^{97}Mo$(n, \gamma)^{98}$Mo measurement is in progress [23]. Also needed are improved data for ^{100}Ru$_{56}$, another key nucleus in the $N = 56$ chain. The information on excitations above 4 MeV in this nucleus is rather scarce and many known levels above 2.5 MeV have only tentative spin-parity assignments.

ACKNOWLEDGMENTS

This work has been supported by the National Science Centre under Contract No. DEC-2018/29/N/ST2/00707. The authors thank the technical services of the ILL, LPSC, and GANIL for supporting the EXILL campaign. The Exogam Collaboration and the INFN Legnaro are acknowledged for the loan of Ge detectors.

[1] A. Kumar and M. R. Gunye, Phys. Rev. C **32**, 2116 (1985).
[2] J. Dobaczewski, in *Contemporary Topics in Nuclear Structure Physics*, edited by R. Casten, A. Frank, M. Moshinski, and S. Pittel (World Scientific, Singapore, 1988), pp. 227–242.
[3] J. Skalski, P.-H. Heenen, and P. Bonche, Nucl. Phys. A **559**, 221 (1993).
[4] T. R. Werner, J. Dobaczewski, M. W. Guidry, W. Nazarewicz, and J. A. Sheikh, Nucl. Phys. A **578**, 1 (1994).

[5] W. Urban, J. L. Durell, A. G. Smith, W. R. Phillips, M. A. Jones, B. J. Varley, T. Rzça-Urban, I. Ahmad, L. R. Morss, M. Bentaleb, and N. Schulz, Nucl. Phys. A **689**, 605 (2001).

[6] W. Urban, T. Rząca-Urban, A. Złomaniec, G. Simpson, J. L. Durell, W. R. Phillips, A. G. Smith, B. J. Varley, I. Ahmad, and N. Schulz, Eur. Phys. J. A **16**, 11 (2003).

[7] W. Urban, J. A. Pinston, J. Genevey, T. Rząca-Urban, A. Złomaniec, G. Simpson, J. L. Durell, W. R. Phillips, A. G. Smith, B. J. Varley, I. Ahmad, and N. Schulz, Eur. Phys. J. A **22**, 241 (2004).

[8] J. Dobaczewski, W. Nazarewicz, J. Skalski, and T. Werner, Phys. Rev. Lett. **60**, 2254 (1988).

[9] R. F. Casten, *Nuclear Structure from a Simple Perspective* (Oxford University Press, Oxford, 1990).

[10] W. Urban, T. Rząca-Urban, J. Wiśniewski, I. Ahmad, A. G. Smith, and G. S. Simpson, Phys. Rev. C **99**, 064325 (2019).

[11] W. Urban, T. Rząca-Urban, A. G. Smith, G. S. Simpson, and J. P. Greene, Phys. Rev. C **102**, 064321 (2020).

[12] W. Urban, K. Sieja, T. Rząca-Urban, J. Wiśniewski, A. Blanc, M. Jentschel, P. Mutti, U. Köster, T. Soldner, G. de France, G. S. Simpson, C. A. Ur, A. G. Smith, and J. P. Greene, Phys. Rev. C **104**, 064309 (2021).

[13] Evaluated Nuclear Structure Data File (ENSDF), https://www.nndc.bnl.gov/ensdf/.

[14] P. Federman and S. Pittel, Phys. Lett. B **69**, 385 (1977); **77**, 29 (1978); Phys. Rev. C **20**, 820 (1979).

[15] P. Federman, S. Pittel, and R. Campos, Phys. Lett. B **82**, 9 (1979).

[16] B. Pritychenko, B. Singh, and M. Verpelli, Nucl. Phys. A **1027**, 122511 (2022).

[17] M. Jentschel, A. Blanc, G. deFrance, U. Köster, S. Leoni, P. Mutti, G. S. Simpson, T. Soldenr, C. A. Ur, W. Urban, and the EXILL Collaboration, J. Instrum. **12**, P11003 (2017).

[18] T. Rząca-Urban, W. Urban, A. Kaczor, J. L. Durell, M. J. Leddy, M. A. Jones, W. R. Phillips, A. G. Smith, B. J. Varley, I. Ahmad, L. R. Morss, M. Bentaleb, E. Lubkiewicz, and N. Schulz, Eur. Phys. J. A **9**, 165 (2000).

[19] A. Blanc, A. Chebboubi, G. de France, F. Drouet, H. Faust, M. Jentschel, G. Kessedjian, U. Köster, S. Leoni, T. Materna, P. Mutti, S. Panebianco, C. Sage, G. S. Simpson, T. Soldner, C. A. Ur, W. Urban, and A. Vancraeyenest, EPJ Web Conf. **93**, 01015 (2015).

[20] C. Michelagnoli, A. Blanc, E. Ruiz-Martinez, A. Chebboubi, H. Faust, E. Froidefond, G. Kessedjian, M. Jentschel, U. Köster, P. Mutti, and G. S. Simpson, EPJ Web Conf. **193**, 04009 (2018).

[21] J. Wiśniewski, W. Urban, T. Rząca-Urban, U. Köster, C. Michelagnoli, M. Jentschel, and P. Mutti, Acta Phys. Pol. B **49**, 547 (2018).

[22] W. Urban, A. Abramuk, A. Blanc, M. Czerwiński, G. de France, M. Jentschel, U. Köster, P. Mutti, T. Rząca-Urban, G. S. Simpson, C. A. Ur, and J. Wiśniewski (unpublished).

[23] J. Wiśniewski, Ph.D. thesis, Warsaw University 2023.

[24] C. M. Baglin, Nucl. Data Sheets **113**, 2187 (2012).

[25] K. Li, J. H. Hamilton, A. V. Ramayya, S. H. Liu, X. Q. Zhang, N. T. Brewer, J. K. Hwang, C. Goodin, S. J. Zhu, Y. X. Luo, J. O. Rasmussen, I. Y. Lee, S. C. Wu, R. Donangelo, A. V. Daniel, G. M. Ter-Akopian, YU. TS. Oganessian, A. Unzhakova, J. D. Cole, W. C. Ma, and M. A. Stoyer, Int. J. Mod. Phys. E **20**, 1825 (2011).

[26] T. Materna, M. Rąpała, A. Letourneau, A. Marchix, O. Litaize, O. Sérot, W. Urban, A. Blanc, M. Jentschel, U. Köster, P. Mutti, T. Soldner, G. Simpson, C. A. Ur, and G. de Freance, EPJ Web Conf. **146**, 04041 (2017).

[27] W. Urban, M. A. Jones, J. L. Durell, M. Leddy, W. R. Phillips, A. G. Smith, B. J. Varley, I. Ahmad, L. R. Morss, M. Bentaleb, E. Lubkiewicz, and N. Schulz, Nucl. Phys. A **613**, 107 (1997).

[28] H. Naïdja, F. Nowacki, B. Bounthong, M. Czerwiński, T. Rząca-Urban, T. Rogiński, W. Urban, J. Wiśniewski, K. Sieja, A. G. Smith, J. F. Smith, G. S. Simpson, I. Ahmad, and J. P. Greene, Phys. Rev. C **95**, 064303 (2017).

[29] M. A. Jones, W. Urban, J. L. Durell, M. Leddy, W. R. Phillips, A. G. Smith, B. J. Varley, I. Ahmad, L. R. Morss, M. Bentaleb, E. Lubkiewicz, and N. Schulz, Nucl. Phys. A **605**, 133 (1996).

[30] T. Rząca-Urban, K. Sieja, W. Urban, M. Czerwiński, A. Blanc, M. Jentschel, P. Mutti, U. Köster, T. Soldner, G. de France, G. S. Simpson, and C. A. Ur, Phys. Rev. C **95**, 064302 (2017).

[31] I. Ahmad and W. R. Phillips, Rep. Prog. Phys. **58**, 1415 (1995).

[32] D. Kameda, T. Kubo, T. Ohnishi, K. Kusaka, A. Yoshida, K. Yoshida, M. Ohtake, N. Fukuda, H. Takeda, K. Tanaka, N. Inabe, Y. Yanagisawa, Y. Gono, H. Watanabe, H. Otsu *et al.*, Phys. Rev. C **86**, 054319 (2012).

[33] D. Abriola and A. A. Sonzogni, Nucl. Data Sheets **109**, 2501 (2008).

[34] D. Pantelica, I. Gh. Stefan, N. Nica, M.-G. Porquet, G. Duchene, A. Astier, S. Courtin, I. Deloncle, F. Hoellinger, A. Bauchet *et al.*, Phys. Rev. C **72**, 024304 (2005).

[35] K. Butler-Moore, J. H. Hamilton, A. V. Ramayya, S. Zhut, X. Zhao, W. C. Ma, J. Kormicki, J. K. Deng, W. B. Gao, J. D. Cole *et al.*, J. Phys. G: Nucl. Part. Phys. **19**, L121 (1993).

[36] J. Chen and B. Singh, Nucl. Data Sheets **164**, 1 (2020).

[37] S. Lalkovski, S. Ilieva, A. Minkova, N. Minkov, T. Kutsarova, A. Lopez-Martens, A. Korichi, H. Hübel, A. Görgen, A. Jansen, G. Schönwasser, B. Herskind, M. Bergström, and Zs. Podolyak, Phys. Rev. C **75**, 014314 (2007).

[38] T. Thomas, K. Nomura, V. Werner, T. Ahn, N. Cooper, H. Duckwitz, M. Hinton, G. Ilie, J. Jolie, P. Petkov, and D. Radeck, Phys. Rev. C **88**, 044305 (2013).

[39] T. Thomas, V. Werner, J. Jolie, K. Nomura, T. Ahn, N. Cooper, H. Duckwitz, A. Fitzler, C. Fransen, A. Gade, M. Hinton, G. Ilie, K. Jessen, A. Linnemann, P. Petkov, N. Pietralla, and D. Radeck, Nucl. Phys. A **947**, 203 (2016).

[40] D. Heck, U. Fanger, W. Michaelis, H. Ottmar, and H. Schmid, Nucl. Phys. A **165**, 327 (1971).

[41] W. Herzog, N. Trautmann, R. Denig, and G. Herrmann, Z. Phys. A **276**, 393 (1976).

[42] H. Mach and R. L. Gill, Phys. Rev. C **36**, 2721 (1987).

[43] R. A. Meyer, J. Lin, G. Molnár, B. Fazekas, A. Veres, and M. Sambataro, Phys. Rev. C **29**, 1839 (1984).

[44] V. Guadilla *et al.*, J. Phys.: Conf. Ser. **1643**, 012134 (2020).

[45] B. C. Rasco, K. P. Rykaczewski, A. Fijałkowska, M. Karny, M. Wolińska-Cichocka, R. K. Grzywacz, D. W. Stracener, E. F. Zganjar, J. C. Batchelder, J. C. Blackmon *et al.*, Phys. Rev. C **105**, 064301 (2022).

[46] K. R. Mashtakov, V. Yu. Ponomarev, M. Scheck, S. W. Finch, J. Isaak, M. Zweidinger, O. Agar, C. Bathia, T. Beck, J. Beller *et al.*, Phys. Lett. B **820**, 136569 (2021).

[47] G. Rusev, R. Schwengner, F. Dönau, S. Frauendorf, L. Käubler, L. K. Kostov, S. Mallion, K. D. Schilling, A. Wagner, E. Grosse, H. von Garrel, U. Kneissl, C. Kohstall, M. Kreutz, H. H. Pitz, M. Scheck, F. Stedile, P. von Brentano, J. Jolie, A. Linnemann *et al.*Phys. Rev. Lett. **95**, 062501 (2005).

[48] J. F. Sharpey-Schafer, S. M. Mulins, R. A. Bark, J. Kau, F. Komati, E. A. Lawrie, J. J. Lawrie, T. E. Madiba, P. Maine, A. Minkova, S. H. T. Murray, N. J. Ncapayi, and P. A. Vymers, Eur. Phys. J. A **47**, 5 (2011).
[49] J. F. Sharpey-Schafer, R. A. Bark, S. P. Bvumbi, T. R. S. Dinoko, and S. N. T. Majola, Eur. Phys. J. A **55**, 15 (2019).
[50] R. A. Meyer, E. Monnand, J. A. Pinston, F. Schussler, B. Pfeiffer, I. Ragnarsson, H. Lawin, G. Lhersonneau, and K. Sistemich, Nucl. Phys. A **439**, 510 (1985).
[51] N. Gavrielov, A. Leviatan, and F. Iachello, Phys. Rev. C **99**, 064324 (2019).
[52] J. E. Garcia-Ramos and K. Heyde, Phys. Rev. C **100**, 044315 (2019).
[53] K. Sieja, Universe **8**, 23 (2022).
[54] K. Sieja, F. Nowacki, K. Langanke, and G. Martinez-Pinedo, Phys. Rev. C **79**, 064310 (2009).
[55] D. Albers, N. Warr, K. Nomura, A. Blazhev, J. Jolie, D. Mücher, B. Bastin, C. Bauerm, C. Bernards, L. Betterman *et al.*, Phys. Rev. Lett. **108**, 062701 (2012).
[56] A. Petrovici and A. S. Mare, Phys. Rev. C **101**, 024307 (2020).
[57] R. A. Meyer, Hyperfine Interact. **43**, 331 (1988).
[58] H. Ohm, M. Linag, G. Molnár, S. Raman, K. Systemich, and W. Unkelbach, Phys. Lett. B **241**, 472 (1990).
[59] Ł. W. Iskra, R. Broda, R. V. F. Janssens, M. P. Carpenter, B. Fornal, T. Lauritsen, T. Otsuka, T. Togashi, Y. Tsunoda, W. B. Walters, and S. Zhu, Phys. Lett. B **788**, 396 (2019).
[60] K. Heyde, P. Van Isacker, R. F. Casten, and J. L. Wood, Phys. Lett. B **155**, 303 (1985).
[61] K. Heyde and J. L. Wood, Rev. Mod. Phys. **83**, 1467 (2011).
[62] G. Molnár, S. W. Yates, and R. A. Meyer, Phys. Rev. C **33**, 1843 (1986).
[63] H. Mach, G. Molnár, S. W. Yates, R. L. Gill, A. Aprahamian, and R. A. Meyer, Phys. Rev. C **37**, 254 (1988).
[64] C. Kremer, S. Aslanidou, S. Bassauer, M. Hilcker, A. Krugmann, P. von Neumann-Cosel *et al.*, Phys. Rev. Lett. **117**, 172503 (2016).
[65] W. Witt, N. Pietralla, V. Werner, and T. Beck, Eur. Phys. J. A **55**, 79 (2019).
[66] D. A. Sazonov, E. A. Kolganova, T. M. Shneidman, R. V. Jolos, N. Pietralla, and W. Witt, Phys. Rev. C **99**, 031304(R) (2019).
[67] E. V. Mardyban, E. A. Kolganova, T. M. Shneidman, R. V. Jolos, and N. Pietralla, Phys. Rev. C **102**, 034308 (2020).
[68] M. L. Stolzenwald, G. Lhersonneau, S. Brant, G. Menzen, and J. Systemich, A. Phys. A **327**, 359 (1987).
[69] F. R. Xu, P. M. Walker, and R. Wyss, Phys. Rev. C **65**, 021303(R) (2002).
[70] W. Urban, T. Rząca-Urban, J. L. Durell, W. R. Phillips, A. G. Smith, B. J. Varley, I. Ahmad, and N. Schulz, Eur. Phys. J. A **20**, 381 (2004).
[71] A. Jalili Majarshin, Y.-A. Luo, F. Pan, and J. P. Draayer, Chin. Phys. C **45**, 024103 (2021).
[72] C. L. Walker, M. Krtička, B. Baramsai, F. Bečvář, T. A. Bredeweg, A. Chyzh, R. C. Haight, M. Jandel, J. Kroll, G. E. Mitchell *et al.*, Phys. Rev. C **92**, 014324 (2015).
[73] M. Sambataro and G. Molnár, Nucl. Phys. A **376**, 201 (1982).
[74] J. A. Shannon, W. R. Phillips, J. L. Durell, B. J. Varley, W. Urban, C. J. Pearson, I. Ahmad, C. J. Lister, L. R. Morss, K. L. Nash, C. W. Williams, N. Schulz, E. Lubkiewicz, and M. Bentaleb, Phys. Lett. B **336**, 136 (1994).
[75] A. Guessous, N. Schulz, W. R. Phillips, I. Ahmad, M. Bentaleb, J. L. Durell, M. A. Jones, M. Leddy, E. Lubkiewicz, L. R. Morss, R. Piepenbring, A. G. Smith, W. Urban, and B. J. Varley, Phys. Rev. Lett. **75**, 2280 (1995).
[76] A. Guessous, N. Schulz, M. Bentaleb, E. Lubkiewicz, J. L. Durell, C. J. Pearson, W. R. Phillips, J. A. Shannon, W. Urban, B. J. Varley, I. Ahmad, C. J. Lister, L. R. Morss, K. L. Nash, C. W. Williams, and S. Khazrouni, Phys. Rev. C **53**, 1191 (1996).
[77] C. L. Zhang, G. H. Bhat, W. Nazarewicz, J. A. Sheikh, and Yue Shi, Phys. Rev. C **92**, 034307 (2015).
[78] K. Nomura, R. Rodríguez-Guzmán, and L. M. Robledo, Phys. Rev. C **94**, 044314 (2016).
[79] H. Abusara, S. Ahmad, and S. Othman, Phys. Rev. C **95**, 054302 (2017).
[80] S. S. Nayak and G. Mukherjee, Nucl. Phys. A **1023**, 122449 (2022).
[81] C. Fransen, N. Pietralla, Z. Ammar, D. Bandyopadhyay, N. Boukharouba, P. von Brentano *et al.*, Phys. Rev. C **67**, 024307 (2003).
[82] S. R. Lesher, C. J. McKay, M. Mynk, D. Bandyopadhyay, N. Boukharouba, C. Fransen, J. N. Orce, M. T. McEllistrem, and S. W. Yates, Phys. Rev. C **75**, 034318 (2007).
[83] D. J. Horen, R. L. Auble, G. R. Satchler, J. R. Beene, I. Y. Lee, C. Y. Wu, D. Cline, M. Devlin, R. Ibbotson, and M. W. Simon, Phys. Rev. C **48**, R2131 (1993).
[84] G. Molnár, H. Ohm, G. Lherssoneau, and K. Systemich, Z. Phys. A **331**, 97 (1988).
[85] K. Nomura, L. Lotina, T. Nikšič, and D. Vretenar, Phys. Rev. C **103**, 054301 (2021).
[86] K. Nomura, Phys. Rev. C **105**, 054318 (2022).
[87] E. T. Gregor, N. N. Arsenyev, M. Scheck, T. M. Shneidman, M. Thurauf, C. Bernards, A. Blanc, R. Chapman, F. Drouet, A. A. Dzhioev *et al.*, J. Phys. G: Nucl. Part. Phys. **46**, 075101 (2019).
[88] T. Rząca-Urban, K. Sieja, W. Urban, F. Nowacki, J. L. Durell, A. G. Smith, and I. Ahmad, Phys. Rev. C **79**, 024319 (2009).
[89] G. S. Simpson, J. A. Pinston, D. Balabanski, J. Genevey, G. Georgiev, J. Jolie, D. S. Judson, R. Orlandi, A. Scherillo, I. Tsekhanovich, W. Urban, and N. Warr, Phys. Rev. C **74**, 064308 (2006).
[90] E. T. Gregor, M. Scheck, R. Chapman, L. P. Gaffney, J. Keatings, K. R. Mashtakov, D. O'Donnell, J. F. Smith, P. Spagnoletti, M. Thürauf, V. verner, and C. Wiesman, Eur. Phys. J. A **53**, 50 (2017).
[91] T. Rząca-Urban, W. Urban, M. Czerwiński, J. Wiśniewski, A. Blanc, H. Faust, M. Jentschel, P. Mutti, U. Köster, T. Soldner, G. de France, G. S. Simpson, and C. A. Ur, Phys. Rev. C **98**, 064315 (2018).